# A review on unitized regenerative fuel cell technologies, part B: Unitized regenerative alkaline fuel cell, solid oxide fuel cell, and microfluidic fuel cell

# A review on unitized regenerative fuel cell technologies, part B: unitized regenerative alkaline fuel cell, solid oxide fuel cell, and microfluidic fuel cell

Yifei Wang[a], Dennis Y.C. Leung[a], Jin Xuan[a,b], Huizhi Wang[a,b]

[a]Department of Mechanical Engineering, The University of Hong Kong, Pokfulam Road, Hong Kong

[b]School of Engineering & Physical Sciences, Heriot-Watt University, Edinburgh EH14 4AS, United Kingdom

Corresponding author: Dennis Y.C. Leung

Tel: (852) 28597911

Fax: (852) 28585415

Email: ycleung@hku.hk

## Abstract

In part A of this review, we have introduced the research progress and application status of unitized regenerative proton exchange membrane fuel cells. In addition to this proton exchange membrane (PEM)-based unitized regenerative fuel cell (URFC), other URFC technologies with different electrolytes have also been reported in the literature, which are the emphasis of this part of review. Unitized regenerative alkaline fuel cells (UR-AFC) have long been utilized for aerospace applications, while the recent development of anion exchange membrane (AEM) has stimulated their further development, especially on the AEM-based UR-AFCs. Vast research works have been reported on the bifunctional oxygen catalyst development, while the latest UR-AFC prototypes are also briefly introduced. Despite of their potential cost-efficiency and better

reactivity, cell performance and round-trip efficiency of the current UR-AFCs are still lower than their PEM-based counterparts. Unitized regenerative solid oxide fuel cell, or more commonly cited as reversible solid oxide fuel cell (RSOFC), is a high-temperature URFC technology with superior performance and reversibility. Review works on this type of URFC are separated into two categories, i.e. RSOFC with oxygen ion conducting electrolyte and RSOFC with proton conducting electrolyte. Even with the highest efficiency among various URFC technologies, the application of RSOFCs, however, is restricted by their limited long-term stability and poor cycle ability. Unitized regenerative microfluidic fuel cell, or called the reversible microfluidic fuel cell, is a newly-emerging URFC research trend which benefits a lot from its membraneless configuration. However, limited research works have been conducted on this new technology.

**Key words**

Unitized regenerative fuel cell, unitized regenerative alkaline fuel cell, reversible solid oxide fuel cell, reversible microfluidic fuel cell

**Abbreviations**

AEM: Anion exchange membrane

AFC: Alkaline fuel cell

BCY: Yttrium-doped barium cerate

BCZY: Yttrium-doped barium cerate zirconate

BCZYbCo: $BaCe_{0.48}Zr_{0.40}Yb_{0.10}Co_{0.02}O_{3-\delta}$

BHC: Bifunctional hydrogen catalyst

BHE: Bifunctional hydrogen electrode

BOC: Bifunctional oxygen catalyst

BOE: Bifunctional oxygen electrode

BOP: Balance of plant

BPPs: Bipolar plates

BSCF: $Ba_{0.5}Sr_{0.5}Co_{0.8}Fe_{0.2}O_{3-\delta}$

BZC: $BaZr_{1-x}Co_xO_{3-\delta}$

EC mode: Electrolysis cell mode

FC mode: Fuel cell mode

GC: Glassy carbon

GDC: Gadolinium-doped ceria

GDL: Gas diffusion layer

gRGO: Gently reduced graphene oxide

HER: Hydrogen evolution reaction

HOR: Hydrogen oxidation reaction

LC: Lanthanum cobaltite

LCC: Lanthanum calcium chromite

LCFCr: $La_{0.3}Ca_{0.7}Fe_{0.7}Cr_{0.3}O_{3-\delta}$

LNO: Lanthanum nickelate

LSC: Lanthanum strontium chromite

LSCF: Lanthanum strontium cobalt ferrite

LSCM: $(La_{0.75}Sr_{0.25})Cr_{0.5}Mn_{0.5}O_3$

LSCN: $La_{2-x}Sr_xCo_{0.5}Ni_{0.5}O_{4\pm\delta}$

LSCuF: Lanthanum strontium copper ferrite

LSF: Lanthanum strontium ferrite

LSGM: Lanthanum strontium gallate magnesite

LSM: Lanthanum strontium manganite

MEMS: Micro-electro-mechanical systems

MFC: Microfluidic fuel cell

MH: Metal hydride

MOF: Metal-organic framework

MWCNTs: Multi-walled carbon nanotubes

NCNTs: Nitrogen-doped carbon nanotubes

N-rGO: Nitrogen-doped reduced graphine oxide

N-rmGO: Nitrogen-doped reduced graphine oxide

N/S-rGO: Nitrogen and sulfur co-doped reduced graphene oxide

OER: Oxygen evolution reaction

ORR: Oxygen reduction reaction

PEM: Proton exchange membrane

PEMFC: Proton exchange membrane fuel cell

PPD: Peak power density

PTFE: Poly Tetra Fluoro Ethylene

qPDTB-$OH^-$: Quaternary ammonium Poly(DMAEMA-co-TFEMA-co-BMA) ionomer

rGO: Reduced graphine oxide

RMFC: Reversible microfluidic fuel cell

RP: Ruddlesden−Popper

RSOFC: Reversible solid oxide fuel cell

RSOFC-H: RSOFCs with proton-conducting electrolyte

RSOFC-O: RSOFCs with oxygen ion-conducting electrolyte

RT-efficiency: Round trip efficiency

ScSZ: Scandia-stabilized zirconia

ScCeSZ: Scandia and ceria stabilized zirconia

SDC: Samaria-doped ceria

SFM: $Sr_2Fe_{1.5}Mo_{0.5}O_{6-\delta}$

SOFC: Solid oxide fuel cell

SOEC: Solid oxide electrolysis cell

SSC: Samarium strontium cobaltite

URFC: Unitized regenerative fuel cell

UR-PEMFC: Unitized regenerative proton exchange membrane fuel cell

UR-AFC: Unitized regenerative alkaline fuel cell

UR-SOFC: Unitized regenerative solid oxide fuel cell

UR-MFC: Unitized regenerative microfluidic fuel cell

UR-PAFC: Unitized regenerative phosphoric acid fuel cell

UR-MCFC: Unitized regenerative molten carbonate fuel cell

WGSR: Water gas shift reaction

YDC: Yttria-doped ceria

YSZ: Yttria-stabilized zirconia

## 1. Introduction

In part-A of this review, we have presented a detailed introduction to the unitized regenerative proton exchange membrane fuel cell (UR-PEMFC), which is currently the most representative and advanced unitized regenerative fuel cell (URFC) technology recorded to date [1-5]. The introduction follows a sequence from the inner cell components, i.e. the bifunctional catalysts, to the outer cell components, i.e. the gas diffusion layer (GDL) and bipolar plates (BPPs). Till now, Pt catalyst is predominantly utilized as bifunctional hydrogen catalyst (BHC), which shows excellent performance in both hydrogen oxidation reaction (HOR) and hydrogen evolution reaction (HER). As for the oxygen electrode, a combination of the best oxygen reduction reaction (ORR) catalyst (i.e. Pt) and oxygen evolution reaction (OER) catalyst (i.e. Ir, Ru and their oxides) is made to prepare bifunctional oxygen catalysts (BOC). Due to the sluggish oxygen reactions [6], cell performance in both fuel cell (FC) and electrolysis cell (EC) mode and the round-trip (RT) efficiency of the present UR-PEMFCs are primarily hindered by oxygen electrode performance. Therefore, numerous research works have been done to optimize BOCs, including their composition, ratio, preparation method, support, binder, and layer structure. As for the GDL and BPPs, research works are mainly focused on their stability improvement, especially in EC mode operation. Furthermore, for practical applications, several systematic issues are carefully investigated to ensure adequate and steady power output, such as heat & water management, electrode configurations, fuel cell stacking, etc. To date, UR-PEMFCs have already been applied in many areas, including aerospace and aviation, renewable energies, grid supplement, transportation, etc. However, due to their relatively high-cost, most applications are still limited to

aerospace and military field. As for civil applications, tentative trials have been conducted to couple this technology with wind & solar energy, power grid, electric vehicles, or employ them as backup powers and uninterrupted power supplies.

Apart from UR-PEMFC, other URFC technologies are also getting more and more R&D interests considering their specific advantages, including the low-temperature unitized regenerative alkaline fuel cell (UR-AFC), high-temperature unitized regenerative solid oxide fuel cell (UR-SOFC), and recently-emerged unitized regenerative microfluidic fuel cell (UR-MFC). To the best of our knowledge, no research works have been reported on either the unitized regenerative phosphoric acid fuel cell (UR-PAFC) or unitized regenerative molten carbonate fuel cell (UR-MCFC) so far.

Compared with the proton exchange membrane (PEM) electrolyte in UR-PEMFC, UR-AFC utilizes either aqueous alkaline solution or anion exchange membrane (AEM) as electrolyte. This alkaline reaction environment provides various benefits such as the improved reaction kinetics and the utilization of non-noble catalysts. However, development of UR-AFC so far is still hindered by either the $CO_2$ poisoning problem or the imperfect AEM [7]. Moreover, the performance and efficiency of present UR-AFCs are also not satisfactory. Different from UR-PEMFC and UR-AFC, UR-SOFC generally works at high temperatures from 500 to 1000℃. Benefiting from this high-temperature effect, outstanding performance and low overpotentials are achievable, while all cell components can be made from cost-efficient ceramic materials. In general, UR-SOFC is very promising for energy storage & conversion purpose in high-temperature environments. However, their stability during regenerative mode operation still needs further improvement. UR-MFC is a recently-emerged URFC technology based on

microfluidic reactors. This kind of device utilizes the interface between two laminar flows as a virtual membrane instead of polymer membranes. Therefore, the fabrication cost is greatly lowered, and the pH environment of both electrodes can be independently tailored to optimize the performance and efficiency [8, 9]. However, UR-MFC generally suffers from poor energy density and difficulties in scalability due to the complex fluid management.

In this part of review, research works related to the above-mentioned three URFC technologies are introduced respectively. For UR-AFC, emphasis will be put on both catalyst and fuel cell development. For UR-SOFC, two mainly types of them, i.e. the oxygen ion-conducting UR-SOFC and the proton-conducting UR-SOFC, are discussed separately, while the related modelling works are also summarized. As UR-MFC is only a newly-emerged technology, only a brief report is given at the present stage.

## 2. Unitized regenerative alkaline fuel cell (UR-AFC)

Alkaline fuel cell (AFC) is one of the most developed fuel cell technologies which has been put into practical services since the early 20th century [7]. During its working process, the conducting ion in the electrolyte is hydroxyl ($OH^-$) moving from cathode to anode, which is similar to proton ($H^+$) moving from anode to cathode in proton exchange membrane fuel cell (PEMFC). As for the electrolyte, either a static porous matrix saturated with aqueous alkaline solution or a flowing aqueous alkaline solution can be adopted. Moreover, recently a new form of electrolyte for AFCs is also developed, namely the AEM, which eliminates the aqueous solution-related problems such as $CO_2$

poisoning and potential electrolyte leakage. However, ionic conductivity and chemical stability of the present AEM is still not as good as its acidic counterpart (i.e. PEM) [7].

UR-AFC, also known as the rechargeable alkaline fuel cell, is developed by combining an alkaline fuel cell with an alkaline electrolyzer into a single unit. One early UR-AFC prototype was proposed in 1960 by Ludwig for the Apollo program [10]. Afterwards, more prototypes were developed by NASA and Giner, Inc. in the 1980s [3]. In the late 1980s, Swette et al. have developed a series of electrocatalysts and catalyst supports for the oxygen electrode of UR-AFCs with good electrochemical activity and stability [11-13]. Recently, research interests are emphasized on the AEM-based UR-AFCs due to their simpler structure and the elimination of possible electrolyte leakage.

Belonging to low-temperature URFCs (20-120℃), one of the most significant advantages of UR-AFC against UR-PEMFC is its ability to use non-noble catalysts instead of the conventional noble metal catalysts, which makes it much more cost-efficient for large-scale manufacture and application. Such non-noble catalysts include nickel or metal hydride for the hydrogen electrode, and transition metal oxides or heteroatom-doped carbon for the oxygen electrode. Another merit of UR-AFC is the improved reaction kinetics in alkaline medium, which helps to improve the sluggish oxygen reaction activity due to the multi-electron transfer processes and strong reaction irreversibility of oxygen [6].

In this section, a brief summary of the latest bifunctional catalysts for both hydrogen and oxygen electrode is given first. Furthermore, recent UR-AFC cell development including performance optimization and stability improvement will also be introduced.

### 2.1 Bifunctional hydrogen catalyst (BHC)

Pt is commonly employed as BHC in UR-PEMFCs because of its high activity towards both HOR and HER. As for UR-AFCs, even though the HOR/HER kinetics on Pt are several orders of magnitude slower in alkaline than in acid medium [14], Pt catalyst with a relatively small loading (e.g. 0.1-1mgcm$^{-2}$) is still competent considering both catalytic activity and cost efficiency [15-18]. Nevertheless, future perspectives of UR-AFCs will still expect non-noble metal based catalysts instead of Pt.

Metal hydrides (MH) can be utilized to fabricate bifunctional hydrogen electrode in UR-AFCs. Such an integrated electrode can not only participate in catalyzing the HOR/HER reaction, but also function as hydrogen storage media. Hu et al. [19] investigated the possibility of an $AB_5$-type MH ($MmNi_{3.88}Co_{0.85}Mn_{0.39}Al_{0.4}$) and a Zr-based $AB_2$-type MH ($ZrNi_{1.2}Mn_{0.48}Cr_{0.28}V_{0.13}$) for hydrogen oxidation and generation, and found that the $AB_5$-type MH exhibited higher HOR and HER activity than the Zr-based $AB_2$-type MH, almost comparable to 10 wt.% Pt/C. In addition to MH, nickel and silver alloy is also considered to be promising as BHC in alkaline medium. Tang et al. [20] synthesized Ni-Ag alloys with various ratios and found that $Ni_{0.75}Ag_{0.25}$ can exhibit 2 times HER activity than pure Ni while with comparable HOR activity.

### 2.2 Bifunctional oxygen catalyst (BOC)

Developing non-noble, highly-active and stable BOC in alkaline medium is not only requisite for UR-AFCs, but also necessary for other energy storage & conversion devices involving the ORR/OER cycling, such as rechargeable metal-air batteries. Great efforts have been made in this area with vast publications, including several related review

papers [6, 21-26]. Since the main interest of this review is not specifically on catalyst progress, therefore, only the latest BOCs in alkaline media will be briefly introduced in this section.

Conventionally, noble metals and their oxides are considered to be the best BOCs with the lowest overpotential. However, for large-scale applications non-noble catalysts are imperative to replace Pt-based noble metal catalysts in UR-AFCs. Among these non-noble catalysts, transition metal oxides, carbonaceous materials and inorganic-organic composites are very promising and have received great investigation in recent literature [23, 26]. In addition, some less-expensive noble metals such as silver were also studied to be appropriate BOC candidates. Moreover, hybrid catalysts comprising two or more of the above-mentioned BOCs were extensively studied to obtain a synergistic effect.

### 2.2.1 Transition metal oxides

Transition metal oxides, especially with the perovskite, pyrochlore, or spinel structures, have long been utilized as electrochemical catalysts for ORR/OER in alkaline media [6]. Recently, vast R&D efforts have been paid to the perovskite and spinel catalysts, while the pyrochlore oxides are less studied [27]. In addition, other transition metal oxides such as the manganese oxides are also found to be effective for the oxygen electro-catalysis.

#### Perovskite oxides

Perovskite oxides generally have the formula of $ABO_3$, where the A site is rare earth or alkali metal ion while the B site is transition metal ion [25]. Despite of their attractive bifunctional catalytic ability, the performance is greatly hindered by their low electrical

conductivity and limited surface area. Nevertheless, the physical-chemical and catalytic properties of perovskite oxides are tunable by changing the composition of the metals. Such a substituted perovskite oxide can generally be described by the formula of $A_{1-x}A'_xB_{1-y}B'_yO_3$ [6]. Zhuang et al. [28, 29] prepared $La_{0.6}Ca_{0.4}CoO_3$ by a modified amorphous citrate precursor method. Compared with the traditional amorphous citrate precursor method, their perovskite exhibited higher surface area and therefore better electro-catalytic activity. Malkhandi et al. [30] also prepared $La_{0.6}Ca_{0.4}CoO_3$ and found that its area-specific catalytic activity increased with the annealing temperature. To increase the electrode surface area, Soares et al. [31] brushed $LaNiO_3$ on a Ni foam substrate, which achieved improved catalytic activity compared with the $LaNiO_3$-pelleted electrode. Takeguchi et al. [16] found that the Ruddlesden-Popper-type layered perovskite, RP-$LaSr_3Fe_3O_{10}$, can function as BOC with almost no overpotentials. This was because of the easily removable oxygen present in RP-$LaSr_3Fe_3O_{10}$. Jung et al. [32] also reported that the doped $La_2NiO_4$ with a layered perovskite structure showed remarkably reduced overpotentials. Jin et al. synthesized $Ba_{0.5}Sr_{0.5}Co_{0.8}Fe_{0.2}O_3$ [33], $Ba_{0.9}Co_{0.5}Fe_{0.4}Nb_{0.1}O_3$ [34] and urchin-like $La_{0.8}Sr_{0.2}MnO_3$ [35] by sol-gel, solid-state reaction and co-precipitation method, respectively. All these perovskites were identified as effective BOCs in alkaline solution. Zhu et al. [36] prepared $LaMO_3$ (M=Fe, Co, Mn) via solution combustion synthesis and found that $LaCoO_3$ was more appropriate as BOC considering both catalytic activity and charge-discharge stability. Zhang et al. [37] improved the bifunctional activity of $LaNiO_3$ by Fe doping, which increased the valence state of the surface Ni. Lopez et al. [38] synthesized $LaMO_3$ (M = Co, Mn, Fe, Ni) by a sol–gel method, among which $LaCoO_3$ achieved the best performance. In addition, partial

substitution of the Ni in $LaNiO_3$ with Mn, Fe, or Co was found to improve the physical and electrochemical properties of the catalyst. Liu et al. [39] developed hierarchical mesporous-macroporous $La_{0.5}Sr_{0.5}CoO_{3-x}$ nanotubes with high surface area via electro-spinning technique, which exhibited outstanding intrinsic ORR and OER catalytic activity. Chen et al. [40] synthesized oxygen-deficient $BaTiO_{3-x}$ by a sol-gel method, which exhibited high bifunctional catalytic activity benefiting from the oxygen vacancies in the perovskite crystal structure. Shim et al. [41] synthesized $LaCoO_3$ fibers with high surface area by calcination of an electrospun polymer-metal precursor fiber, which showed better electrochemical properties than $LaCoO_3$ powders. Stoerzinger et al. [42] investigated the role of strain and conductivity in perovskite BOC activity, which was helpful to the rational design of highly active catalyst. Oh et al. [43]synthesized $La_{0.6}Sr_{0.4}CoO_{3-\delta}$ by the Pechini method, which showed much better electro-catalytic activity than the Ketjen black. For more details of the perovskite oxide BOCs, readers are referred to a recent review by Gupta et al. [25]

**Spinel oxides**

Spinel oxides generally have the formula of $AB_2O_4$, where the A site and B site are both transition metal ions. Among all the spinel BOCs, cobaltite such as $Co_3O_4$ and $NiCo_2O_4$ have received the most attention, which was reviewed by Hamdani et al. [21] in 2010. Ever since then, continuous research efforts have been paid to develop efficient, stable and low-cost spinel catalysts. Cheng et al. [44] prepared nano-crystalline $Co_xMn_{3-x}O_4$ under room temperature rapidly by reduction of amorphous $MnO_2$ precursors in an aqueous solution containing $Co^{2+}$. The as-prepared catalyst outperformed the high-

temperature prepared $Co_xMn_{3-x}O_4$ due to its high surface areas and abundant defects. Kong [45] prepared rod and bead-like $Co_3O_4$ via a method of chemical synthesis in combination with calcinations under different temperatures. It was found that the bead-like $Co_3O_4$ had better bifunctional activity than the rod-like $Co_3O_4$. Jin et al. [46] prepared $NiCo_2O_4$ spinel nanowire arrays with high specific surface area through a facile template-free co-precipitation route. The catalyst has promising catalytic activity for ORR and OER, as well as excellent stability and reversibility. Sa et al. [47] synthesized meso-porous $Co_3O_4$ by nano-casting, which showed enhanced activity and stability over the $Co_3O_4$ prepared by hydrothermal method. This could be attributed to its high surface area and structural stability. Prabu et al. [48] prepared hierarchical nanostructured 1-D $NiCo_2O_4$ by electro-spinning, which showed remarkable electro-catalytic activity towards ORR and OER. Maiyalagan et al. [49] developed $LiCoO_2$ with a lithiated spinel structure (LT-$LiCoO_2$) by solid-state reaction, which was an efficient electrocatalyst for OER but had poor activity for ORR. However, the chemically delithiated LT-$Li_{1-x}CoO_2$ was found to be highly active for both ORR and OER. Menezes et al. [50] prepared porous $CoMn_2O_4$ and $MnCo_2O_4$ microspheres by the thermal degradation of respective carbonate precursors as BOC. It was found that the cubic $MnCo_2O_4$ exhibited better OER activity while the tetragonal $CoMn_2O_4$ performed better in ORR. They also synthesized $Co_3O_4$ nanochains by low-temperature degradation of a cobalt oxalate precursor, which showed excellent OER activity and comparable ORR activity with Pt/C [51]. Xu et al. [52] prepared $CoFe_2O_4$ hollow nanospheres by hydrothermal method. Superior bifunctional catalytic activity as well as excellent stability was achieved, which could be attributed to its special 3-D hierarchical porous structure. In addition, $MnCo_2O_4$ by sol-gel process

[53], $Ni_xCo_{3-x}O_4$ films by electro-deposition [54] and $CuCo_2O_4$ by a sacrificial support method [55] were also proposed in recent literature.

**Manganese oxides**

Manganese oxides ($MnO_x$) have long been considered as fine catalysts for ORR or OER [56]. Recently it has been found that some phases of $MnO_x$ can exhibit bifunctional catalytic activity. Gorlin et al. [57] prepared $MnO_x$ thin film on glassy carbon substrate by electro-deposition, which showed excellent ORR/OER activity similar to Pt, Ru and Ir, and the oxidation state of Mn(III) was confirmed. They also found that a heat treatment under 450 or 500℃ can enhance its bifunctional catalytic activity [58]. Pickrahn et al. [56] proposed an atomic layer deposition method to prepare $MnO_x$ on glassy carbon followed by an annealing process. The as-prepared catalyst showed a conformal thin film structure and was comparable to the best $MnO_x$ catalysts in the literature. Selvakumar et al. [59] investigated the effect of nano-shapes on the catalytic activity of α-$MnO_2$. It was found that the nano-wire $MnO_2$ exhibited enhanced electro-catalytic activity compared with the nano-tube and nano-particle $MnO_2$. Chen et al. [60] studied the effect of Ir-doping on $MnO_x$ activity. With an increasing Ir content, the ORR activity first increased and then decreased, while the OER activity was considerably improved with only a small amount of Ir doping. Meng et al. [61] synthesized $MnO_x$ of various structures (α, β, δ-$MnO_2$ and amorphous) and found that the electro-catalytic activities are strongly dependent on the crystallographic structures, which followed an order of α-$MnO_2$ > amorphous > β-$MnO_2$ > δ-$MnO_2$.

### 2.2.2 Carbonaceous materials

Carbon-based materials have been widely employed as effective catalyst support in fuel cell electrodes for many years. Recently, heteroatom-doped (e.g. N, S, B or P) carbon nanomaterials were found to possess promising bifunctional oxygen catalytic ability. These metal-free BOCs have attracted extensive research interests due to their reasonable balance between cost, catalytic activity, electronic conductivity, surface area, and abundance [24]. Lin et al. [62] prepared N-doped graphene by the pyrolysis of graphene oxide and polyaniline. Cheng et al. [63] doped boron into multi-walled carbon nanotubes (B-MWCNTs) by thermal annealing MWCNTs in the presence of boric acid. Wang et al. [64]synthesized N-doped graphene via a hydrothermal method with ammonia as the nitrogen precursor. Zhang et al. [65] doped nitrogen and phosphorus into mesoporous nano-carbon foam by the pyrolysis of a polyaniline aerogel synthesized in the presence of phytic acid. Vineesh et al. [66] prepared B-doped graphene derived from the rhombohedral boron carbide. Yadav et al. [67] synthesized bamboo-shaped carbon nitrogen nanotubes with different diameter distribution by a liquid chemical vapor deposition technique. Li et al. [68] prepared 2-D microporous carbon sheets derived from eggplant via carbonization and KOH activation. He et al. [69] doped nanocarbon-intercalated graphene with nitrogen and iron. Yuan et al. [70] prepared the N-doped activated carbon sheets which was derived from chitin by a facile and cost-favorable heat treatment. Lee et al. [71] synthesized 3-D mesoporous graphene from a Ni(II) molecular coordination compound. Li et al. [72] prepared the N,P co-doped graphene/carbon nanosheets with N,P-doped carbon sandwiching few-layers-thick graphene. Hadidi et al. [73] prepared hollow N-doped mesoporous carbon spheres via polymerization and

carbonization of dopamine. Qu et al. [74] doped nitrogen and sulfur into mesoporous carbon nanosheets on the basis of graphene oxide-polydopamine hybrids. All these carbon-based metal-free BOCs were reported to demonstrate outstanding bifunctional catalytic activity and good stability, which could be benefited from the heteroatom doping effect, large surface area, excellent electronic conductivity, etc.

### 2.2.3 inorganic-organic composites

In addition to the above-mentioned inorganic catalysts, inorganic-organic composites are also investigated as possible BOC candidates in alkaline media. These organometallic complexes are generally composed of metal center and organic matrix, such as the transition metal macrocycles and metal–polymer composites [23]. Yin et al. [75] embedded α-$MnO_2$ nanoparticles in porous chromium terephthalate matrix (MIL-101(Cr)) using a hydrothermal method, which can improve both the catalytic activity and stability. They also utilized MIL-101(Cr) to support the cobalt catalyst by an impregnation process [76]. Wang et al. [77] prepared a mixed metal-ion metal-organic framework (MOF) via hydrothermal method. Ferric and cobalt salts were used as metal-ion precursors and trimesic acid as the organic ligand. The as-prepared MOF (Fe/Co) achieved a high specific surface area and excellent bifunctional catalytic activity. Cao et al. [78] modified the surface of $MnCo_2O_4$ with polypyrrole to improve its electronic conductivity. The as-prepared hybrid exhibited comparable bifunctional activity with commercial Pt/C and $RuO_2$/C but with much higher stability. Roy et al. [79] prepared several organometallic complexes based on Ni, Co, Cu, or Fe, in which the metals were immobilized by ligands

and covalently attached to carbon black. After a one-step pyrolysis, decent activities towards ORR/OER were achieved compared with the 30% Pt/C.

### 2.2.4 Silver catalyst

Although belonging to noble metals, silver is approximately 100 times less expensive than platinum, and has high electrical conductivity, competent catalytic activity, and a longer lifetime. Therefore, some researchers studied silver or silver-based materials as BOCs. Sasikala et al. [80] prepared Ag nano-powder as BOC in alkaline media by wet chemical method, which showed promising characteristics towards ORR and OER. Yang et al. [81] fabricated nano-porous Ag-embedded $SnO_2$ thin film by anodic treatment of electro-deposited Ag−Sn alloy layers. This highly porous structure greatly improved the roughness factor, providing more electro-catalytically active sites for the oxygen reactions. Jin et al. [82] grew Ag-Cu dendrites on Ni foams via a two-step galvanic displacement reaction, which demonstrated excellent performance and stable cycle ability.

### 2.2.5 Hybrid catalysts

To improve the bifunctional catalytic activity and durability, two or more of the above-mentioned BOCs can be coupled together as hybrid catalysts to achieve a synergistic effect. Vast research outcomes have been reported in this field to find effective and cost-efficient catalyst combinations, including the hybrids of transition metal oxide – carbon, transition metal oxide – noble metal, transition metal oxide – transition metal oxide, etc. Figure-1 shows SEM images of some hybrid catalysts with various combinations and structures. In this section, only a brief summary of these hybrid catalysts is provided.

**Transition metal oxide - carbon**

Spinel oxides have been extensively utilized in this combination considering their outstanding bifunctional activity, such as the $Co_3O_4$ [83-92], $Co_xMn_yO_4$ [93-99], $Co_xFe_yO_4$ [100, 101], $CoMnFeO_4$ [102], $CoMnNiO_4$ [103], $Mn_3O_4$ [86], etc. Perovskite oxides were also frequently employed to couple with carbon, such as the $LaNiO_3$ [104-106], $BaMnO_3$ [107], Co-doped $LaMnO_3$ [108, 109], $Ba_{0.5}Sr_{0.5}Co_{0.8}Fe_{0.2}O_{3-\delta}$ [110], $La(Co_{0.55}Mn_{0.45})_{0.99}O_{3-\delta}$ [108], $(La,Sr)CoO_3$ [111], $La_{0.5}Sr_{0.5}Co_{0.8}Fe_{0.2}O_3$ [112], etc. In addition, other metal oxides such as the $MnO_x$ [89, 113-115], $CoO_x$ [116, 117], $NiO_x$ [89, 116] were investigated in the literature, while some transition metal sulfides [118-121] were also applicable in this combination.

As for the carbon component, many options were available including the graphitized carbon [114, 121], carbon nanotubes [84, 89, 97, 100, 103, 104, 106, 109, 112, 113, 115, 122], graphene [83, 87, 93, 117, 119], reduced graphene oxide [94, 95, 98, 101, 102, 108, 111, 120, 123], etc. Moreover, these carbon components are generally doped with nitrogen, sulfide, or co-doped with them to improve their catalytic activity.

**Transition metal oxide – noble metal**

Noble metal alone is not suitable for BOC fabrication in alkaline medium due to its high cost and poor abundance. However, it can be coupled with non-noble catalysts with a relatively low content, among which silver is especially attractive considering its low cost, high electrical conductivity and satisfactory catalytic activity. Several works have been done to couple silver with various transition metal oxides, including $FeAgMo_2O_8$

[124], $La_{0.6}Ca_{0.4}CoO_3$ [125], $MnO_2$ [126], $Co_3O_4$ [127, 128], etc. In addition, platinum [129-131] and gold [132] were also investigated for this type of hybrid catalyst.

**Transition metal oxide – transition metal oxide**

Some researchers coupled two different transition metal oxides together and found that the hybrid catalyst outperformed both of its components alone. Such combinations include the $Co_3O_4$ - $MnO_2$ [133], $Co_3O_4$ - $Co_2MnO_4$ [134], $La_{0.8}Sr_{0.2}MnO_{3-\delta}$ - $Ba_{0.5}Sr_{0.5}Co_{0.8}Fe_{0.2}O_{3-\delta}$ [135], $MnO_2$ - $LaNiO_3$/$LaCoO_3$ [136], $MnO_2$ - $LaCoO_3$/$Nd_3IrO_7$ [137], etc.

**Transition metal – carbon**

In addition to the oxides, transition metal nanoparticles were also utilized to couple with carbonaceous materials as hybrid catalysts, among which the cobalt nanoparticles were most commonly employed [138-143]. Other metals such as iron and nickel nanoparticles were also investigated in the literature [141, 142].

**2.3 Cell development**

UR-AFCs were first proposed and manufactured for aviation and aerospace purpose due to their distinct advantage in power output and energy density. Various NASA patents concerning this technology were filed since 1960s. However, their development gradually slowed down later on, while research interests were transferred to UR-PEMFCs with solid PEM electrolyte. Recently, with the development of non-noble electrocatalysts

and AEM electrolyte, interests on UR-AFCs have returned considering their potential cost superiority and improved reaction kinetics against UR-PEMFCs.

### 2.3.1 Carbon-free electrode

GDL plays very important roles in electrodes, which provides both supporting substrate and gas channels for the catalyst layer. In conventional AFCs, carbon papers or carbon cloths are commonly employed as GDL. For UR-AFCs, however, carbon materials can be easily corroded at high potentials in EC mode, leading to a poor stability. Figure-2 shows a carbon paper-based oxygen electrode with severe corrosion after 200 cycles' operation in alkaline environment. To solve this problem, carbon-free GDLs such as nickel foam [144-146], Au-coated titanium mesh [18] and stainless steel substrate [17, 147, 148] are normally utilized instead for oxygen electrode fabrication.

### 2.3.2 AEM-based URFC prototypes

A UR-AFC based on AEM is very fascinating compared with its aqueous alkaline electrolyte-based counterpart. Several latest prototypes with either commercial or home-made AEMs were proposed recently, which were summarized in Table-1 with their performance, efficiency and stability compared. However, till now the reported UR-AFC performances and RT-efficiencies are still lower than those in UR-PEMFCs.

Wu et al. [15] developed a UR-AFC with Pt/C as BHC and Cu, Mn-incorporated $Co_3O_4$ as BOC. The electrolyte was a home-made AEM. After coating the catalysts onto the opposite sides of the membrane using an air-brush, two carbon papers were used to sandwich the MEA and functioned as current collector. However, this cell only achieved

moderate performance, i.e. a peak power density (PPD) of 80mWcm$^{-2}$ under 40℃, mainly due to the low ionic conductivity of the AEM. To solve this problem, Wu et al. [18] developed a new AEM by filling the pores of a porous PTFE with an anion exchange ionomer (qPDTB-OH$^{-}$). This new AEM can be ultrathin thus leading to a much lower resistance. UR-AFC prototype utilizing this AEM achieved a higher PPD of 163mWcm$^{-2}$ at 45℃, even with a lower anode catalyst loading. As for the stability, this cell was charged at 100mAcm$^{-2}$ for nearly 200hrs with degradation rate of 0.0379mVh$^{-1}$ for the first 120hrs, showing satisfying durability possibly attributed to the Au-coated titanium mesh as GDL for oxygen electrode.

For large-scale applications, future UR-AFC systems should totally get rid of the noble metal-based catalysts in both electrodes. Ng et al. [149] first proposed such a noble metal-free UR-AFC prototype with Ni/C as BHC, a mixture of Ni/C and $MnO_x$/Glassy-carbon as BOC, and a commercial AEM as electrolyte. However, tested under 65℃, PPD of only 16.5mWcm$^{-2}$ was achieved. RT-efficiency at 10mAcm$^{-2}$ was 40% at the beginning, but dropped to 34% after 8 charge-discharge cycles, which might be due to the carbon materials used as catalyst support and GDL. To improve the stability, a stainless steel mesh was employed instead of the carbon catalyst support [17]. This time the UR-AFC achieved significantly enhanced durability for 10 cycles.

The strong irreversibility of ORR/OER in oxygen electrode causes high overpotentials during both discharge and charge processes, leading to poor reversibility and low energy efficiency. Takeguchi et al. developed a UR-AFC prototype with much lower overpotentials in both modes, as shown in Figure-3. Such high energy efficiency was

benefited from the novel BOC, i.e. the RP-$LaSr_3Fe_3O_{10}$, which showed much lower overpotentials than the $RuO_2$-$IrO_2$ and $LaMnO_3$/$LaNiO_3$ catalyst.

UR-AFCs can also be microminiaturized as on-chip power sources in micro-electro-mechanical systems (MEMS). Bretthauer et al. [150] fabricated a micro-scale UR-AFC as a micro-accumulator for energy harvesting purpose in an autonomous MEMS. This micro cell employed $LaNi_5$-based MH as hydrogen electrode and storage, AEM as electrolyte and deposited Pt as air-breathing oxygen electrode. A PPD of 0.559mWcm$^{-2}$ was achievable. However, the sputtered Pt thin-film electrode failed to provide sufficient electro-catalytic surface for the oxygen reaction, and the use of precious metal is not cost-efficient. In another paper, Bretthauer et al. [151] replaced Pt with $La_{0.6}Ca_{0.4}CoO_3$/C which was sprayed on a perforated Ni membrane as air-breathing electrode. This precious-metal free micro UR-AFC achieved a PPD of 0.66mWcm$^{-2}$ and very stable performance in both modes.

## 3. Reversible Solid Oxide Fuel Cell (RSOFC)

Solid oxide fuel cell (SOFC) is a kind of high temperature fuel cell. Unlike PEMFC or AFC which generally operates below 200℃, intermediate-temperature SOFC [152] usually works in the range of 500-750℃, and high-temperature SOFC [153] works in the range of 750-1000℃. Benefiting from this temperature advantage, SOFC can utilize hydrocarbons directly as fuel, and earth-abundant non-precious materials for fabricating its cell components such as the electrolyte and electrodes. Moreover, the reaction activity and energy efficiency are also improved [154-158].

A SOFC can be reversely operated for fuel generation purpose, namely the solid oxide electrolysis cell (SOEC). SOEC shares many similarities with SOFC, including high temperature operation, electrolyte and electrode material, and cell structure etc. Moreover, one extraordinary feature of SOEC against other water electrolysis technologies is its ability to utilize heat input to decrease the electrical consumption when producing fuel. As shown in Figure-4, the overall energy demand during SOEC operation is insensitive to temperature. Therefore, a temperature rise can significantly decrease the electrical energy demand by increasing the thermal energy demand [154], leading to a much higher electrical-to-chemical energy efficiency which can even exceed 100% [159]. However, direct operation of SOFC as SOEC can bring several long-term stability problems due to the different electrical potential gradient and reaction environment between these two reverse processes [160].

Since the structure and materials are very similar between SOFC and SOEC, it is obvious that a solid oxide cell can alternatively work in FC and EC mode. Such a device is called the UR-SOFC, or more commonly cited as reversible solid oxide fuel cell (RSOFC) in the literature [152, 153, 160]. Pioneer works on the reversibility of RSOFC were presented by Erdle et al.[161] for tubular cells, and by Shimaki et al.[162] and Kusunoki et al. [163] for planar cells. Afterwards, more and more research efforts have been paid on this technology, including several related review papers [5, 154-158, 164]. However, as mentioned earlier, the material and structural degradation is still a great challenge for the practical application of RSOFC. Due to the high temperature regenerative operation, conventional electrolyte/electrode materials may be no longer

appropriate, demanding for a further investigation for more suitable materials for the FC/EC operations.

According to the electrolyte type, the existing RSOFCs can be divided into two main categories: RSOFC with oxygen ion-conducting electrolyte (RSOFC-O) [152, 153, 160, 163, 165-195], and RSOFC with proton-conducting electrolyte (RSOFC-H) [196-200]. In addition, an innovative RSOFC with mixed protonic-anionic conducting dual-electrolyte was presented recently by Viviani et al. [201] despite of its moderate performance, while a co-ionic conducting electrolyte which can simultaneously conduct $H^+$ and $O^{2-}$ during the operation was also reported by Zheng et al. [202] In this section, recent R&D efforts on these two types of RSOFCs will be introduced separately, while modelling works will also be briefly introduced.

### 3.1 RSOFC with oxygen ion conducting electrolyte (RSOFC-O)

To date, RSOFC-O is the mainstream of RSOFC study due to the abundant research experience on oxygen-ion conducting electrolyte-based SOFCs and SOECs, and its superior performance compared with RSOFC-H [158]. Preliminary test of a RSOFC-O based on conventional SOFC materials was done by Kusunoki et al. [163] and good reversibility between FC and EC mode was verified. However, it is well-known that RSOFCs based on conventional materials usually achieve poorer performance and stability in EC mode than in FC mode. Therefore, great efforts have been done on material optimization for different cell components, which will be discussed in detail below. In addition, other research works related to RSOFC-O are also introduced,

including stability study and systematic issues such as stacking, cell structure, and syngas operation.

Table-2 summarizes RSOFC-O prototypes demonstrated to date since the 1990s, including the electrode and electrolyte materials, PPD and stability. Due to their possibility of reverse mode operation, the existing SOFCs and SOECs in the literature can actually be treated as potential RSOFCs. However, only the research works including cell operation in both modes are reviewed here.

### 3.1.1 Material optimization

#### Electrolyte

Typical oxygen ion conducting electrolytes include yttria-stabilized zirconia (YSZ), scandia-stabilized zirconia (ScSZ), doped lanthanum gallate such as the Sr, Mg-doped $LaGaO_3$ (LSGM), and some ceria-based oxides such as the samaria-doped ceria (SDC) and gadolinium-doped ceria (GDC) [154]. Among all these materials, YSZ is currently the most popular electrolyte for RSOFC development, as indicated in Table-2.

Same as in the cases of SOFCs and SOECs, YSZ is still the most utilized electrolyte material for RSOFC-O due to its good thermal and chemical stability, high oxygen ion conductivity, and fine mechanical strength at high temperature (800-1000℃) [169]. Both thick YSZ pellet (0.5-1mm) [163, 165-168, 176, 180] and thin YSZ membrane (<100μm) [174, 175, 177, 178] have been employed for the electrolyte-supported and electrode-supported RSOFC-Os, respectively, and have achieved satisfactory performance in both modes. Fan et al. [188] employed a thin YSZ electrolyte (20-30μm) and achieved a PPD of 0.9$Wcm^{-2}$ at 800℃. However, Bercero et al. [153] found that YSZ electrolyte can be

reduced at high electrolysis potentials, leading to an irreversible damage to the YSZ-oxygen electrode interface. In addition to yttria, other dopants such as scandia and ceria were also employed for zirconia as RSOFC-O electrolyte material, such as the ScSZ [190, 192] and ScCeSZ [152, 181].

Zirconia-based electrolyte is competent for high temperature operation (800-1000℃), while other electrolyte materials such as the doped lanthanum gallate and ceria-based oxides are more suitable for intermediate temperature operation (500-800℃) [154]. Lanthanum gallate typically doped by Sr and Mg, i.e. the LSGM, is a very promising electrolyte material which is compatible with Co-based perovskites. However, LSGM is known to be incompatible with nickel-based fuel electrode, which is the best hydrogen electrode material till now. Elangovan et al. [172] found that by using Ni-MgO instead of Ni, the reactivity between gallate electrolyte and hydrogen electrode is lowered. Ceria-based electrolytes are effective in lowering the electrode polarization, but the reduction of $Ce^{4+}$ to $Ce^{3+}$ at high applied voltage leads to serious stability problems [154]. In order to prevent the reduction process, composite electrolyte composed of both a SDC/GDC layer and a thin YSZ layer were proposed [160, 173, 187, 189, 191, 193].

**Bifunctional hydrogen electrode (BHE)**

As shown in Table-2, Ni blended with the corresponding electrolyte material is currently the most utilized BHE due to its low cost, high electrochemical reactivity, and high electronic conductivity [169]. However, Ni can be easily oxidized during electrolysis operation, which demands for a portion of hydrogen gas input together with the steam in EC mode. In addition, the poor redox cycle ability of Ni will cause volume

instability (coarsening of Ni particles) [169, 185]. Nevertheless, research works on BHE are still mainly focused on the optimization of Ni-based electrode, especially on its structural optimization. Momma et al. [166] found the asymmetric behavior of Ni-YSZ electrode in FC & EC modes, indicating the existence of a diffusion-limited process in EC mode operation, even though the cell is electrolyte-supported. As for hydrogen electrode-supported cell, the asymmetric behavior would be much severer due to the mass transfer resistance of steam. To solve this problem, a two-layer electrode structure was proposed with a thin Ni-YSZ functional layer and a thick Ni-YSZ support layer [158], as shown in Figure-5(b). The thin functional layer has micro-pores for better contact with the electrolyte layer while the thick support layer has macro-scale pores for better mass transport. Ni et al. [203] also studied the effect of this micro-structurally graded electrode, and found it beneficial to mass transport but with negligible effects on the ohmic and activation overpotentials, especially for thick electrodes. Compared with conventional electrode with uniform porosity and particle size as shown in Figure-5(a), this micro-structurally graded electrode showed significantly higher power density in FC mode operation. Choi et al. [185] found that an extra porous Ni-YSZ layer between the hydrogen electrode and electrolyte can improve the cell performance due to the improved diffusion of reactive species inside the electrode. Yoon et al. [191] optimized the poor structure of hydrogen electrode by using poly(methyl methacrylate) (PMMA) as pore-forming agent. Consequently, the hydrogen production rate in EC mode is improved by a factor greater than two.

Conventionally, Ni-YSZ electrode is fabricated by mixing Ni powder with electrolyte slurry followed by a sintering process. Instead, a novel fabrication method is proposed by

depositing the Ni catalyst into a porous scaffold which is made of the electrolyte material. This novel method was reported to be helpful in overcoming the Ni agglomeration problem. Uchida et al. [168] dispersed nm-sized Ni catalysts into a porous SDC scaffold. The electrode exhibited stable performance at 0.6Acm$^{-2}$ and 800℃ for over 1100hrs. Cable et al. [179] infiltrated Ni nitrates into YSZ scaffold and then decomposed the nitrates into metallic Ni by heat treatment. As shown in Figure-6, no obvious evidence of Ni agglomeration was found after the electrolysis operation. Chen et al. [192] also deposited Ni-SDC into YSZ scaffold as BHE by an impregnation method. After been charged at 166mAcm$^{-2}$ and 600℃ for more than 300hrs, cell performance was significantly increased probably due to the reorganization of particles or the slight decrease in OCV.

**Bifunctional oxygen electrode (BOE)**

For BOE fabrication, lanthanum strontium manganite (LSM) is widely applied in RSOFC-Os, which has decent oxygen catalytic property, high electronic conductivity, low ionic conductivity, low reactivity with YSZ, and thermal expansion coefficient close to YSZ [187]. To increase the triple phase boundary and reaction sites, a mixture of LSM and YSZ is usually utilized instead of LSM alone. Despite of these merits, LSM-YSZ electrode is found to be less stable in EC mode than in FC mode, which causes degradation problems in regenerative operation [165]. Instead of LSM, mixed ion- and electron-conducting materials (MIEC) such as lanthanum strontium ferrite (LSF), lanthanum strontium copper ferrite (LSCuF), and lanthanum strontium cobalt ferrite (LSCF) are proposed which generally show lower overpotential losses and better

catalytic activities. However, these materials suffer from high reactivity with YSZ electrolyte at high temperatures [173]. Other BOE materials were also developed to improve the stability status, especially for EC mode operation. Bercero et al. [152] employed $La_{2-x}Sr_xCo_{0.5}Ni_{0.5}O_{4\pm\delta}$ (LSCN) as oxygen electrode with ScCeSZ as electrolyte. The cell performed equally in FC and EC mode with very close ASR values, indicating a good reversibility possibly attributed to the flexible oxygen non-stoichiometry of LSCN. Rao et al. [184] used $Sm_{0.5}Sr_{0.5}CoO_{3-\delta}$ (SSC) blended with SDC electrolyte material as oxygen electrode. Even though SSC has excellent surface oxygen exchange rate, electrical conductivity and bulk oxygen ion diffusion coefficient, its high cost and lack of the thermal compatibility has hindered the application [160]. To solve this problem, Lee et al. [160] impregnated the SSC catalyst into a porous LSCF-GDC composite backbone as oxygen electrode. Other oxygen electrode materials such as $Nd_2O_3$-$Nd_2NiO_{4+\delta}$ [192] are less studied in the literature.

### 3.1.2 Stability study

It is well known that the long-term performance degradation is much faster for a SOEC than a SOFC [157]. Similarly, a RSOFC generally faces inferior stability in EC mode than in FC mode [190]. As shown in Figure-7, the major causes to RSOFC single cell degradation include Ni particle agglomeration [204], Si-containing impurities from glass sealants [174], oxygen electrode delamination [190, 205] , YSZ electrolyte reduction [153], etc. As for RSOFC stack, Cr-poisoning from the metallic interconnects should also be considered.

Hauch et al. [174] operated their RSOFC in EC mode and found that the voltage degradation rate was 2%/1000h at 500mAcm$^{-2}$ under 850℃, which was higher than in FC mode with similar cells. The main reason for this degradation is the increased loss of hydrogen electrode, even though no electrode porosity change or delamination from the electrolyte was found. However, Si-containing impurities were found in the hydrogen electrode which may partially block the reaction sites. Schiller et al. [175] tested their metal-supported RSOFC in EC mode at 300mAcm$^{-2}$ under 800℃ and the degradation rate was 3.2%/1000h. Possible reasons behind this degradation include oxidation of the metal-support, and Ni coarsening in the BHE.

While some researchers focus on the study of RSOFC stability in EC mode, stability problems in alternative regenerative mode operation may be a more pressing challenge. Figure-8 compares several cycle test results of RSOFCs from different research groups, which shows unsatisfactory cycle stability in (a)-(c), while better results are achieved in (d) and (e). Cable et al. [179] found their cell degraded much faster in regenerative mode operation with a rate around 30%/1000h in both modes. Choi et al. [185] found that the successive regenerative mode operation has brought great challenge to the cell reversibility, which was mainly caused by the grain growth in oxygen electrode. Hong et al. [190] applied LSC as oxygen electrode to a 3-cell stack, which faced rapid degradation in regenerative mode operation within 5 cycles (140h). Crack formation and delamination at the electrolyte-barrier layer interface were responsible for this rapid degradation. Same phenomenon was also mentioned by Fan et al. [189] whose cell also encountered rapid degradation after 13 regenerative cycles (26h), which was also attributed to the delamination of the barrier layer from the electrolyte. Fan et al. [188]

also tried to infiltrate LSCF powder into the porous YSZ backbone as oxygen electrode, however, the agglomeration of LSCF particles will lead to instability during the FC-EC regenerative cycles. Even with so many reports on regenerative mode instability, there was one encouraging result reported by McElroy et al. [171] Their RSOFC has been demonstrated for over 1000 hours with stable operation in regenerative mode, and the degradation rate of RT-efficiency was as low as 0.5%/1000h.

Matsui et al. [167] studied the RSOFC stability under limited fuel condition in FC mode and limited steam condition in EC mode to simulate the gas environment at the downstream part of the cell when high fuel utilization was required. They found that a much faster degradation occurred than those under sufficient fuel and steam conditions, indicating the trade-off between fuel utilization and long-term stability of RSOFCs in practical applications.

Yoo et al. [195] proposed the use of lanthanum nickelate, $La_2NiO_{4+\delta}$ (LNO) as oxygen electrode and believed that its ability to accommodate excess oxygen species in interstitial positions can help to mitigate the electrode-electrolyte delamination problem. However, only the FC mode long-term stability was confirmed in their experiment, while the stability in EC mode remained to be seen.

### 3.1.3 Systematic development

#### Stacking

To obtain practical voltage and power output, RSOFC single cells need to be stacked together while separated by interconnects between each two cells. Both short stacks with several cells [186, 190] and long stacks with 25-100 cells [171, 172] have been proposed

in the literature. As for interconnects, metallic-based plates with flow fields curved on both sides are commonly employed, which functions similarly to the BPPs in UR-PEMFC stacks. In addition, Cable et al. [179] have developed a thin, Ca-doped $LaCrO_3$ interconnect instead of conventional metal interconnects, which can not only improve the system energy density, but also greatly mitigate the Cr poisoning effect compared with metallic interconnects. Figure-9 exhibits several RSOFC stack prototypes reported to date, including the NASA all-ceramic stack by Cable et al. [179], Jülich 2-cell stack by Nguyen et al. [186], and a 200W-class 3-cell stack by Hong et al. [190]

Stack degradation tends to be faster than single cell degradation probably due to the extra influences from the piping, interconnects and sealing [186]. Nguyen et al. tested a 2-cell stack for 8000 hours in total under both constant FC mode and EC mode operation. Degradation rate of 0.6%/1000h was achieved in FC mode, while negligible degradation was found in EC mode operation at lower current density. However, the degradation increased when the electrolysis current density increased from 300 to 875$mAcm^{-2}$ [186]. Elangovan et al. [172] tested an 8-cell stack in FC mode and found that the degradation rate was as high as 20% per 1000h, which was mainly due to the Cr evaporation from the metal interconnects. By replacing the ferritic stainless steel with nickel-based super-alloy as interconnects to alleviate Cr evaporation, the stack achieved much better stability in EC mode for about 150hrs. Hong et al. [190] fabricated a 3-cell RSOFC stack with metallic interconnects. Tested under 750℃ in FC mode, the stack achieved a power output of 200W at 2.2V and 90.9A, while the cell ASR in EC mode was found to be comparable to that in FC mode. The stack also exhibited quite stable performance in EC

mode with a low degradation rate of 7.75% per 1000h. However, similar to RSOFC single cells, alternative regenerative operation of the stack will lead to fast degradation.

**Symmetrical RSOFC**

Symmetrical fuel cells utilize the same catalytic material for both electrodes, which is applicable not only to SOFCs/SOECs but also to RSOFCs as long as the material itself is redox reversible [155]. Symmetrical RSOFCs hold several advantages against the conventional RSOFCs, such as reduced strains during manufacture, ease of co-sintering, and lower fabrication cost [169]. Bastidas et al. [169] employed $(La_{0.75}Sr_{0.25})Cr_{0.5}Mn_{0.5}O_3$ (LSCM) perovskite as symmetrical electrode for RSOFC. The cell achieved a PPD of $0.3Wcm^{-2}$ at 900℃, and the ASR values are very close in two modes, i.e. $0.78\Omega cm^{-2}$ in FC mode and $0.84\Omega cm^{-2}$ in EC mode, indicating a fine reversibility. Molero-Sanchez et al. [194] found that the mixed-conducting perovskite oxide, $La_{0.3}Ca_{0.7}Fe_{0.7}Cr_{0.3}O_{3-\delta}$ (LCFCr), is suitable for symmetrical electrode fabrication. During the reversible operation, LCFCr electrode showed very good stability with little loss in performance, and no interfacial damage was observed. Liu et al. [206, 207] utilized $Sr_2Fe_{1.5}Mo_{0.5}O_{6-\delta}$ (SFM) perovskite as symmetrical electrode. In FC mode, OCV was 1.07V and PPD reached $835mWcm^{-2}$ at 900℃, while in EC mode an electrolysis current of $0.88Acm^{-2}$ and a hydrogen production rate of $380mlcm^{-2}h^{-1}$ were achieved at 1.3V. Furthermore, the cell has demonstrated stable performance in EC mode at 1.2V for 100hrs.

**Planar vs. tubular RSOFC**

Similar to SOFCs and SOECs, both planar and tubular RSOFCs have been proposed in the literature, while the tubular type is far less studied than the planar cells. In addition, the size of these tubular RSOFCs is usually very small, i.e. with an active area from 2cm$^2$ [153] to 7.5cm$^2$ [182], which is also called the micro-tubular RSOFC. Figure-10 shows a typical micro-tubular RSOFC prototype. The inside fuel electrode layer (pink) is much thicker than the middle electrolyte layer (red) and outside oxygen electrode layer (blue), which serves as the support for the whole cell, while Ni mesh on the electrode surface serves as current collector. Compared with planar cells, micro-tubular RSOFCs achieve several advantages such as higher power density per unit volume, rapid thermal cycling, easy sealing, and less redox cycling damage [153].

**Syngas operation**

In addition to the "$H_2$-$H_2O$" cycle, RSOFC is also possible with the "hydrocarbon fuel-$CO_2$" cycle benefiting from its high temperature operation, which is commonly known as the syngas operation. As shown in Figure-11, hydrocarbon fuels such as $CH_4$ or methanol can be directly utilized to produce electricity in FC mode. In EC mode, $CO_2$ waste and steam can be co-electrolyzed to produce syngas (CO-$H_2$ mixture) first, and the syngas can then be converted to either $CH_4$ or liquid hydrocarbon fuels through the methanation reaction (Eq. (1)) or the Fischer-Tropsch reaction (Eq. (2)), respectively. RSOFCs with the "hydrocarbon fuel-$CO_2$" cycle hold several advantages against the conventional "$H_2$-$H_2O$" cycle, such as easier fuel storage and transportation, higher RT-efficiency etc. [177]

$$CO + 3H_2 \leftrightarrow CH_4 + H_2O \qquad (1)$$

$$nCO + (2n+1)H_2 \leftrightarrow C_nH_{(2n+2)} + nH_2O \qquad (2)$$

Zhan et al. [177] studied the co-electrolysis of $CO_2$-$H_2O$-$H_2$ to produce syngas. Operated on 25% $CO_2$, 25% $H_2O$ and 50% $H_2$ at 800℃ and 1.3V, syngas production rate of 7sccm $cm^{-2}$ was yielded. Compared with pure $H_2O$ electrolysis, pure $CO_2$ electrolysis was much slower, while the $H_2O$-$CO_2$ co-electrolysis rate was only slightly decreased. They also found that the cathodic reactions are probably dominated by $H_2O$ reduction, while CO is mainly produced via the reverse water gas shift reaction (WGSR) instead of direct $CO_2$ reduction [178]. Ni [208] also found that the reversible methanation and reforming reactions are not favored in $H_2O$-$CO_2$ co-electrolysis, while the WGSR can significantly influence the co-electrolysis behavior. Moreover, it was found that the reversible WGSR contributed to CO production at a low operating potential while consuming CO at a high operating potential, which also depended on the operating temperature and inlet gas composition [209].

Stability problem with syngas operation may be quite different from those utilizing pure $H_2$ and steam. Lohsoontorn et al. [180] studied the durability of Ni-YSZ hydrogen electrode under various gas environments. They found that Ni-YSZ was very stable in $H_2O$ electrolysis condition and in $H_2O$-$CO_2$ co-electrolysis condition, while significant degradation occurred when $CO_2$ electrolysis was carried out. Nguyen et al. [186] also found that the degradation rate of $H_2O$-$CO_2$ co-electrolysis is only slightly higher than $H_2O$ electrolysis.

### 3.2 RSOFC with proton-conducting electrolyte (RSOFC-H)

Compared with RSOFC-O, research works on RSOFC-H so far are much less, but with great potential for energy conversion applications under intermediate temperatures (500-

700℃). By employing a proton-conducting electrolyte, steam is provided to the BOE side during EC mode operation, therefore producing pure hydrogen in the BHE side without further need of hydrogen separation [197]. In addition, a potentially higher energy efficiency can be achieved with a proton conducting electrolyte [210], and the lower activation resistance of RSOFC-H makes it very suitable for intermediate temperature operation, which is advantageous in material selection and cell fabrication [197]. Furthermore, the configuration dilemma between BHE-support and BOE-support structure is no longer a problem for RSOFC-H, since the BHE-support structure favors both FC & EC mode operation [197]. All these advantages of RSOFC-H make it a fascinating and promising technology for energy conversion purpose at intermediate temperature range. However, more R&D efforts should be paid on its performance improvement, electrode optimization, and long-term stability before any practical applications.

Since Iwahara et al. [211] first applied $SrCeO_3$ as proton conducting electrolyte for water electrolysis in 1981, more and more proton-conducting materials were developed for SOFCs and SOECs, such as the doped $BaZrO_3$, $BaCeO_3$, and $SrZrO_3$ [200]. Among them, $BaCeO_3$ is most widely utilized, but its thermodynamic instability against $H_2O$ and $CO_2$ has hindered its further application [200]. Compared with $BaCeO_3$, the $BaZrO_3$-based electrolyte is chemically stable against $H_2O$ and $CO_2$, but has very poor sinterability for electrolyte fabrication [196]. One eclectic solution is to introduce Zr into $BaCeO_3$ to enhance its chemical stability. Under this strategy, the yttrium-doped barium cerate zirconate (BCZY) becomes one of the most promising proton-conducting material

which shows both high conductivity and chemical stability under $H_2O/CO_2/H_2S$-containing environment [197, 199, 200].

Table-3 summarizes several RSOFC-H prototypes reported to date, including electrolyte and electrodes materials, operating temperature, PPD, and stability studies. As mentioned earlier, BCZY is widely employed for electrolyte fabrication due to its good performance and stability. For BHE, Ni blended with electrolyte material is still predominant which is similar to the case in RSOFC-O. As for BOE, some RSOFC-Hs employed the same material as RSOFC-Os such as LSC [198] and SSC [197], while others utilized particular materials such as $BaZr_{1-x}Co_xO_{3-\delta}$ (BZC) [199] or $Ba_{0.5}Sr_{0.5}Co_{0.8}Fe_{0.2}O_{3-\delta}$ (BSCF) [200]. To inhibit the oxygen ion conductivity of the electrolyte, intermediate temperature from 500 to 700℃ is generally applied. Under this temperature range, PPD as high as $493mWcm^{-2}$ was achieved at 600℃ by Yoo et al. [200] as shown in Figure-12. However, RSOFC-H still generally provides lower power output than RSOFC-O. This might be due to the un-optimized electrode material and micro-structures such as the porosity, pore size, tortuosity etc. [158, 210], which induces great research potential in the future.

In addition to performance disadvantage, the long-term and regenerative stability is also an important issue for RSOFC-H. Rao et al. [199] operated their cell at 1.3V in EC mode and achieved quite stable result for 5hrs, while Yoo et al. [200] found their cell relatively stable at $300mAcm^{-2}$ in FC mode for 600hrs. Nonetheless, no long-term EC mode tests or regenerative mode tests are available till now, which calls for further investigations.

### 3.3 Modelling works

Mathematical modelling is a cost-effective method for RSOFC design and parametric optimization. Moreover, it can provide a deep-going understanding of the fundamental mechanisms during RSOFC operation [212]. Ni et al. analyzed the concentration overpotentials of RSOFCs with either an oxygen-ion conducting electrolyte [213] or a proton conducting electrolyte [214, 215]. For RSOFC-O in EC mode operation, high concentration overpotential occurred in the BHE side which restricts cell performance, while in FC mode the high concentration overpotential occurred in the BOE side. This concentration overpotential discrepancy in two modes has brought a configuration dilemma to RSOFC-O as mentioned earlier. However, this dilemma is eliminated for RSOFC-H because the high concentration overpotential occurred in the BOE side in both modes, which favors the hydrogen-electrode support configuration. Moyer et al. [182] developed a model for RSOFC with syngas operation. They found that the combination of hydrogen- and oxygen-spillover mechanisms provided a better representation of situations involving $H_2$-CO electro-oxidation and $H_2O$-$CO_2$ electrolysis. Su et al. [216] developed a 2-D axisymmetric model for button cells and found a great fuel concentration gradient near the electrolyte-electrode interface. They also found that the temperature and electrode porosity have a beneficial effect on RSOFC performance attributed to the enhanced electrochemical reactions and species mass transfer [217]. García-Camprubí et al. [218] reviewed the fitting process of the electrochemical parameters in the existing SOFC, SOEC and RSOFC modelling works, and concluded that this process was not clearly explained or sufficiently justified. They found that the charge transfer coefficients are not always equal to 0.5, which can be more accurate by

thorough and careful fitting, and the value of exchange current density depended on the reactant concentration. They also introduced a comprehensive model for RSOFC simulation together with a detailed fitting process of the electrochemical parameters. Kazempoor et al. [219] integrated a SOFC model with a SOEC model to form a general RSOFC model. Cell behavior under various conditions can be precisely simulated by this model with proper fitting parameters. With this model, various operating parameters were investigated, such as the operating temperature, gas composition, flow rate and pressurized operation, etc.

Most of the RSOFC modelling works focused on steady-state operation, while Jin et al. [212] studied the RSOFC modelling in switching-mode operation. They developed a 2-D transient mathematical model to study the changes of various parameters during the mode-switch period, such as the ionic and electronic potentials, mass fraction distribution of $H_2/O_2/H_2O$, etc.

For practical applications such as the distributed energy storage and conversion, the implementation of a RSOFC system must be considered, which may bring extra design challenges on system configuration and operation conditions. Wendel et al. [220, 221] studied the thermal management strategy for a RSOFC system through both experimental and modelling works. By utilizing carbonaceous reactant species and adopting intermediate temperature operation, the RSOFC system was able to be thermally self-sustained in EC mode. Moreover, trade-offs between electric efficiency, thermal management, energy density and durability were also found. Ren et al. [222] studied the integration of a RSOFC system with a power electronic invertor for distributed power storage/generation purpose. In a discharge-charge cycle, the maximum energy storage

efficiency was calculated to be 64%. In addition, the trade-off between two invertor control algorithms was also investigated.

## 4. Reversible microfluidic fuel cell (RMFC)

Since its first appearance in 2002 [223], microfluidic fuel cell (MFC) has received numerous R&D attentions due to its distinctive advantages such as cost-effectiveness, easy fabrication, elimination of membrane-related problems, flexible pH adjustment etc. [8]. A MFC is the kind of device which utilizes two laminar flows in parallel to deliver fuel and oxidant to the anode and cathode respectively, with all components confined in a microfluidic channel [8]. During the operation, flow interface in the middle of the channel serves as a virtual membrane to separate fuel and oxidant and to transfer ions. Figure-13 shows some common cell structures of MFC [9], including the T-shape channel with electrodes on the channel bottom, T-shape channel with electrodes on the two channel sides, F-shape channel with an air-breathing cathode, and a specific structure with flow-through electrodes for vanadium species. To date, various types of fuel, including vanadium redox species [224-226], hydrogen [227, 228], methanol [229, 230], ethanol and formic acid [231-233], have been applied in MFC, while great efforts have been made on their power output, fuel utilization [234, 235], stacking [236, 237], fuel cycling [238], etc. In addition, modelling works were also reported to better understand the electrochemical mechanism of this technology [239-244].

RMFC is a new concept which endows MFC the ability to reproduce fuel in EC mode. Figure-14 illustrates how a typical air-breathing RMFC system works. In FC mode, fuel and electrolyte are pumped through the cell and $O_2$ is supplied from the ambient air,

while the generated $CO_2$ and remaining electrolyte are stored in separate reservoirs. During EC mode, the $CO_2$ and electrolyte are pumped back to the cell for electrolysis reaction to re-generate the fuel and release $O_2$ to the ambient. Feasibility of this concept is first experimentally investigated by Kjeang et al. [226] in a vanadium RMFC with flow-through porous electrodes. During the charge mode, $V^{2+}$ and $VO^{2+}$ are regenerated by pumping waste solution back to the channel and applying an electrolytic voltage. In this way, the RMFC works similarly to redox flow batteries. In addition to vanadium, hydrogen and hydrocarbon fuel reproduction is also possible with this technology. Hydrogen production via water electrolysis is a common process for most URFCs and may be especially advantageous for RMFC considering its pH adjustment ability. As for hydrocarbon fuels such as formic acid and methanol, this research trend shows enormous importance for building a carbon neutral energy conversion cycle [245]. Whipple et al. [246] developed a RMFC for the reduction of $CO_2$ to formic acid. It was found that an acidic pH environment could lead to a significant increase in faradaic and energetic efficiencies, which can reach 89% and 45% at $100 mA cm^{-2}$, respectively. Xuan et al. [247] developed a computational model to study the effect of pH on RMFC performance especially on BOE side, and they also found that RMFC favors acidic operation. In order to find out the limiting factors to RMFC performance, Wang et al. [248] developed a numerical model for microfluidic fuel cell mainly on the electrolytic direction. It was found that the low diffusivity of $CO_2$ in the GDE and the dilution effect of HER hindered the cell performance and efficiency improvement. In conclusion, RMFC development to date is still on its early stage but with great potentials, which requires more research and insight in the future.

## 5. Applications and challenges

Compared with UR-PEMFC, reported applications of UR-AFC and RSOFC are very scarce, while RMFC is far away from its application stage. Therefore, in this section only a brief introduction to their application potentials and challenges is presented.

UR-AFC is first proposed for aerospace applications during the 1960s. Afterwards, more protoypes were developed by NASA and Giner, Inc. However, interests in this technology then dropped due to technical and economic factors, while the UR-PEMFC technology seemed more appealing and received more R&D attentions. Recently with the development of AEM, technical problems such as $CO_2$ poisoning of the BOE and potential electrolyte leakage are solved. Therefore, the application potential of UR-AFC is rediscovered considering its non-noble catalyst employment and high reaction kinetics. Nevertheless, cell performance and energy efficiency of the present UR-AFCs are still lower than those of UR-PEMFCs, while the best AEM is not competitive against PEM considering both conductivity and stability. In addition, despite of the potential cost reduction benefited from cheaper catalysts and membrane, systematic costs derived from other cell components such as the GDL, BPPs, etc. and from the system balance of plants (BOPs) may also be obstacles for their large-scale commercialization.

RSOFC technology is much younger than either UR-PEMFC or UR-AFC, which favors a high temperature working environment. During the regenerative operation, a variety of power sources can be utilized to provide thermal energy to RSOFC, such as nuclear power, wind/solar energy, and waste heat from high-temperature industrial processes. Same as UR-PEMFC, RSOFC can also be utilized in aerospace, terrestrial, and

portable applications, but at reduced capital costs. Benefiting from the non-noble ceramic materials utilized for both electrolyte and electrode fabrication, RSOFC is very cost-efficient compared with other types of URFC, while the cell performance and energy efficiency is also very high. The major obstacle hindering the wide-application of RSOFC is the long-term stability problem especially during frequent regenerative operations. Moreover, the cost of the high-temperature fabrication process and the heat management sub-system during practical operation also need to be considered when competing with other energy storage & conversion technologies.

As for RMFC, the low-cost fabrication and adjustable reaction environment make this technology very promising compared with its membrane-based counterparts. However, the complex fluid management in the stacking process together with the potentially leakage of acid/alkaline electrolyte can be a serious problem. In addition, RMFC for portable applications may be a difficult task considering the laminar-flow interface stability in the micro-channels.

## 6. Conclusion

In this part of review, research progress on various URFC technologies are introduced separately, including the UR-AFC, RSOFC and RMFC. For UR-AFC, a brief introduction to the bifunctional hydrogen and oxygen catalyst is given first, together with some UR-AFC prototypes based on AEM. It is worth to mention that the listed BOCs here are not only applicable to UR-AFC, but also useful in other energy conversion devices with aqueous alkaline electrolyte, such as rechargeable metal-air battery. For RSOFC, researches are separated into two parts according to the different electrolyte

materials utilized, i.e. the oxygen ion conducting electrolyte and the proton-conducting electrolyte. RSOFC is best known for its high temperature operation and therefore high energy efficiency. In this review, emphasis is put on the material aspect and stability study. Moreover, modelling works on RSOFC is also reported. As for RMFC, due to the limited research works available, only a few preliminary studies are presented here.

Based on the two parts of this URFC technology review, several conclusions to the above-mentioned four types of URFC can be made as follows:

- Considering the power output ability, both UR-PEMFC and RSOFC-O achieve very high PPD around 1-2$Wcm^{-2}$, while the RSOFC-H, UR-AFC and RMFC generally achieve lower PPD less than 500$mWcm^{-2}$.
- Considering the RT-efficiency, RSOFC exhibits superior advantage against the other three URFC technologies, which is even comparable with secondary batteries. As for UR-PEMFC, UR-AFC and MFC, lower efficiency (less than 50%) is normally achieved.
- Considering the cycle stability, recorded tests with UR-PEMFC generally shows better stability than those with RSOFC and UR-AFC. As for RMFC, no cycle test is found yet.
- Considering the cost-efficiency, UR-PEMFC is much more expensive than the other URFC technologies due to its inevitable usage of noble-metal catalyst and high-cost Nafion membrane. While for RMFC, obvious cost superiority is confirmed benefiting from its membraneless configuration, flexible pH environment thus wide catalyst choice, and the low-cost fabrication process.

Right now, URFC has shown its tremendous application prospects in both aerospace and terrestrial areas. Benefiting from its high energy density, deep cycling ability, and the decoupled energy storage capacity & rated power, URFC has exhibited superior advantages for long-term energy storage and power output purpose. However, till now only the UR-PEMFC reaches an early-application stage. As for the other types of URFC, unsatisfactory performance and poor cycle ability are the two main problems for UR-AFC, while RSOFC generally suffers from stability problem especially in the EC mode. As for RMFC, development is still on a very early stage with various unsolved problems. Nevertheless, considering the cost and scarcity of noble metal catalysts, these three types of URFC are very promising as long as continuous efforts are paid.

**Acknowledgement**

This project is supported by the Hong Kong Research Grant Council CERG #714313.

**References:**

[1] Pettersson J, Ramsey B, Harrison D. A review of the latest developments in electrodes for unitised regenerative polymer electrolyte fuel cells. Journal of Power Sources. 2006;157:28-34.

[2] Dihrab SS, Sopian K, Alghoul MA, Sulaiman MY. Review of the membrane and bipolar plates materials for conventional and unitized regenerative fuel cells. Renewable and Sustainable Energy Reviews. 2009;13:1663-8.

[3] Müller M. Regenerative Fuel Cells. Fuel Cell Science and Engineering: Materials, Processes, Systems and Technology. 2012:219-45.

[4] Gabbasa M, Sopian K, Fudholi A, Asim N. A review of unitized regenerative fuel cell stack: Material, design and research achievements. International Journal of Hydrogen Energy. 2014;39:17765-78.

[5] Millet P. Unitized Regenerative Systems. Hydrogen Production: Electrolysis. 2015:167-90.

[6] Jörissen L. Bifunctional oxygen/air electrodes. Journal of Power Sources. 2006;155:23-32.

[7] Merle G, Wessling M, Nijmeijer K. Anion exchange membranes for alkaline fuel cells: A review. Journal of Membrane Science. 2011;377:1-35.

[8] Kjeang E, Djilali N, Sinton D. Microfluidic fuel cells: A review. Journal of Power Sources. 2009;186:353-69.

[9] Goulet M-A, Kjeang E. Co-laminar flow cells for electrochemical energy conversion. Journal of Power Sources. 2014;260:186-96.

[10] Ludwig FA. Energy conversion cell. Google Patents; 1964.

[11] Swette L, Giner J. Oxygen electrodes for rechargeable alkaline fuel cells. Journal of Power Sources. 1988;22:399-408.

[12] Swette L, Kackley N. Oxygen electrodes for rechargeable alkaline fuel cells - II. Journal of Power Sources. 1990;29:423-36.

[13] Swette L, Kackley N, McCatty SA. Oxygen electrodes for rechargeable alkaline fuel cells. III. Journal of Power Sources. 1991;36:323-39.

[14] Sheng W, Gasteiger HA, Shao-Horn Y. Hydrogen Oxidation and Evolution Reaction Kinetics on Platinum: Acid vs Alkaline Electrolytes. Journal of The Electrochemical Society. 2010;157:B1529-B36.

[15] Wu X, Scott K. A non-precious metal bifunctional oxygen electrode for alkaline anion exchange membrane cells. Journal of Power Sources. 2012;206:14-9.

[16] Takeguchi T, Yamanaka T, Takahashi H, Watanabe H, Kuroki T, Nakanishi H, et al. Layered Perovskite Oxide: A Reversible Air Electrode for Oxygen Evolution/Reduction in Rechargeable Metal-Air Batteries. Journal of the American Chemical Society. 2013;135:11125-30.

[17] Ng JWD, Tang M, Jaramillo TF. A carbon-free, precious-metal-free, high-performance O2 electrode for regenerative fuel cells and metal-air batteries. Energy & Environmental Science. 2014;7:2017-24.

[18] Wu X, Scott K, Xie F, Alford N. A reversible water electrolyser with porous PTFE based OH− conductive membrane as energy storage cells. Journal of Power Sources. 2014;246:225-31.

[19] Hu W-K, Noréus D. Metal hydrides as bi-functional catalysts for hydrogen generation and oxidation in reversible MH-air fuel cells. Electrochemistry Communications. 2009;11:2212-5.

[20] Tang MH, Hahn C, Klobuchar AJ, Ng JWD, Wellendorff J, Bligaard T, et al. Nickel-silver alloy electrocatalysts for hydrogen evolution and oxidation in an alkaline electrolyte. Physical Chemistry Chemical Physics. 2014;16:19250-7.

[21] Hamdani M, Singh R, Chartier P. Co3O4 and Co-based spinel oxides bifunctional oxygen electrodes. Int J Electrochem Sci. 2010;5:556-77.

[22] Zhang T, Imanishi N, Takeda Y, Yamamoto O. Aqueous lithium/air rechargeable batteries. Chemistry Letters. 2011;40:668-73.

[23] Cheng F, Chen J. Metal–air batteries: from oxygen reduction electrochemistry to cathode catalysts. Chemical Society Reviews. 2012;41:2172-92.

[24] Li Q, Cao R, Cho J, Wu G. Nanocarbon electrocatalysts for oxygen reduction in alkaline media for advanced energy conversion and storage. Advanced Energy Materials. 2014;4.

[25] Gupta S, Kellogg W, Xu H, Liu X, Cho J, Wu G. Bifunctional Perovskite Oxide Catalysts for Oxygen Reduction and Evolution in Alkaline Media. Chemistry–An Asian Journal. 2015.

[26] Narayan S, Manohar A, Mukerjee S. Bi-Functional Oxygen Electrodes–Challenges and Prospects. The Electrochemical Society Interface. 2015;24:65-9.

[27] Abreu-Sepulveda M. Diverse Pyrochlore Materials for Oxygen Reduction and Evolution Reaction in Alkaline Medium. 225th ECS Meeting (May 11-15, 2014): Ecs; 2014.

[28] Zhuang S, Huang C, Huang K, Hu X, Tu F, Huang H. Preparation of homogeneous nanoporous La0.6Ca0.4CoO3 for bi-functional catalysis in an alkaline electrolyte. Electrochemistry Communications. 2011;13:321-4.

[29] Zhuang S, Zhang H, Liu S, Tu F, Zhang W, Zhao C. Optimized Perovskite Electrocatalyst for Bifunctional Air Electrode by Impedance Spectroscopy Analysis. Int J Electrochem Sci. 2014;9:1690-701.

[30] Malkhandi S, Yang B, Manohar AK, Manivannan A, Prakash GKS, Narayanan SR. Electrocatalytic Properties of Nanocrystalline Calcium-Doped Lanthanum Cobalt Oxide for Bifunctional Oxygen Electrodes. The Journal of Physical Chemistry Letters. 2012;3:967-72.

[31] Soares CO, Carvalho MD, Melo Jorge ME, Gomes A, Silva RA, Rangel CM, et al. High surface area LaNiO3 electrodes for oxygen electrocatalysis in alkaline media. Journal of Applied Electrochemistry. 2012;42:325-32.

[32] Jung K-N, Jung J-H, Im WB, Yoon S, Shin K-H, Lee J-W. Doped Lanthanum Nickelates with a Layered Perovskite Structure as Bifunctional Cathode Catalysts for Rechargeable Metal–Air Batteries. ACS Applied Materials & Interfaces. 2013;5:9902-7.

[33] Jin C, Cao X, Lu F, Yang Z, Yang R. Electrochemical study of Ba 0.5 Sr 0.5 Co 0.8 Fe 0.2 O 3 perovskite as bifunctional catalyst in alkaline media. International Journal of Hydrogen Energy. 2013;38:10389-93.

[34] Jin C, Yang Z, Cao X, Lu F, Yang R. A novel bifunctional catalyst of Ba0. 9Co0. 5Fe0. 4Nb0. 1O3Ld perovskite for lithiumeair battery. international journal of hydrogen energy. 2014;39:e2530.

[35] Jin C, Cao X, Zhang L, Zhang C, Yang R. Preparation and electrochemical properties of urchin-like La0.8Sr0.2MnO3 perovskite oxide as a bifunctional catalyst for oxygen reduction and oxygen evolution reaction. Journal of Power Sources. 2013;241:225-30.

[36] Zhu C, Nobuta A, Nakatsugawa I, Akiyama T. Solution combustion synthesis of LaMO3 (M = Fe, Co, Mn) perovskite nanoparticles and the measurement of their electrocatalytic properties for air cathode. International Journal of Hydrogen Energy. 2013;38:13238-48.

[37] Zhang D, Song Y, Du Z, Wang L, Li Y, Goodenough JB. Active LaNi 1− x Fe x O 3 bifunctional catalysts for air cathodes in alkaline media. Journal of Materials Chemistry A. 2015;3:9421-6.

[38] Lopez K, Park G, Sun H-J, An J-C, Eom S, Shim J. Electrochemical characterizations of LaMO3 (M= Co, Mn, Fe, and Ni) and partially substituted LaNi x M1− x O3 (x= 0.25 or 0.5) for oxygen reduction and evolution in alkaline solution. Journal of Applied Electrochemistry. 2015;45:313-23.

[39] Liu G, Chen H, Xia L, Wang S, Ding L-X, Li D, et al. Hierarchical Mesoporous/Macroporous Perovskite La0. 5Sr0. 5CoO3–x Nanotubes: A Bifunctional Catalyst with Enhanced Activity and Cycle Stability for Rechargeable Lithium Oxygen Batteries. ACS applied materials & interfaces. 2015;7:22478-86.

[40] Chen C-F, King G, Dickerson RM, Papin PA, Gupta S, Kellogg WR, et al. Oxygen-deficient BaTiO 3− x perovskite as an efficient bifunctional oxygen electrocatalyst. Nano Energy. 2015;13:423-32.

[41] Shim J, Lopez K, Sun H-J, Park G, An J-C, Eom S, et al. Preparation and characterization of electrospun LaCoO3 fibers for oxygen reduction and evolution in rechargeable Zn–air batteries. Journal of Applied Electrochemistry. 2015;45:1005-12.

[42] Stoerzinger KA, Choi WS, Jeen H, Lee HN, Shao-Horn Y. Role of Strain and Conductivity in Oxygen Electrocatalysis on LaCoO3 Thin Films. The Journal of Physical Chemistry Letters. 2015;6:487-92.

[43] Oh MY, Jeon JS, Lee JJ, Kim P, Nahm KS. The bifunctional electrocatalytic activity of perovskite La 0.6 Sr 0.4 CoO 3− δ for oxygen reduction and evolution reactions. RSC Advances. 2015;5:19190-8.

[44] Cheng F, Shen J, Peng B, Pan Y, Tao Z, Chen J. Rapid room-temperature synthesis of nanocrystalline spinels as oxygen reduction and evolution electrocatalysts. Nat Chem. 2011;3:79-84.

[45] Kong F. Synthesis of rod and beadlike Co3O4 and bi-functional properties as air/oxygen electrode materials. Electrochimica Acta. 2012;68:198-201.

[46] Jin C, Lu F, Cao X, Yang Z, Yang R. Facile synthesis and excellent electrochemical properties of NiCo 2 O 4 spinel nanowire arrays as a bifunctional catalyst for the oxygen reduction and evolution reaction. Journal of Materials Chemistry A. 2013;1:12170-7.

[47] Sa YJ, Kwon K, Cheon JY, Kleitz F, Joo SH. Ordered mesoporous Co 3 O 4 spinels as stable, bifunctional, noble metal-free oxygen electrocatalysts. Journal of Materials Chemistry A. 2013;1:9992-10001.

[48] Prabu M, Ketpang K, Shanmugam S. Hierarchical nanostructured NiCo 2 O 4 as an efficient bifunctional non-precious metal catalyst for rechargeable zinc–air batteries. Nanoscale. 2014;6:3173-81.

[49] Maiyalagan T, Jarvis KA, Therese S, Ferreira PJ, Manthiram A. Spinel-type lithium cobalt oxide as a bifunctional electrocatalyst for the oxygen evolution and oxygen reduction reactions. Nature communications. 2014;5.

[50] Menezes PW, Indra A, Sahraie NR, Bergmann A, Strasser P, Driess M. Cobalt–Manganese-Based Spinels as Multifunctional Materials that Unify Catalytic Water Oxidation and Oxygen Reduction Reactions. ChemSusChem. 2015;8:164-71.

[51] Menezes PW, Indra A, González-Flores D, Sahraie NR, Zaharieva I, Schwarze M, et al. High-Performance Oxygen Redox Catalysis with Multifunctional Cobalt Oxide Nanochains: Morphology-Dependent Activity. ACS Catalysis. 2015;5:2017-27.

[52] Xu Y, Bian W, Wu J, Tian J-H, Yang R. Preparation and electrocatalytic activity of 3D hierarchical porous spinel CoFe 2 O 4 hollow nanospheres as efficient catalyst for

Oxygen Reduction Reaction and Oxygen Evolution Reaction. Electrochimica Acta. 2015;151:276-83.

[53] Cao X, Jin C, Lu F, Yang Z, Shen M, Yang R. Electrochemical Properties of MnCo2O4 Spinel Bifunctional Catalyst for Oxygen Reduction and Evolution Reaction. Journal of The Electrochemical Society. 2014;161:H296-H300.

[54] Lambert TN, Vigil JA, White SE, Davis DJ, Limmer SJ, Burton PD, et al. Electrodeposited Ni x Co 3− x O 4 nanostructured films as bifunctional oxygen electrocatalysts. Chemical Communications. 2015;51:9511-4.

[55] Serov A, Andersen N, Matanovic I, Roy A, Atanassov P. Oxygen Reduction and Oxygen Evolution Electrocatalysts Prepared By Sacrificial Support Method (SSM). Meeting Abstracts: The Electrochemical Society; 2015. p. 1957-.

[56] Pickrahn KL, Park SW, Gorlin Y, Lee H-B-R, Jaramillo TF, Bent SF. Active MnOxElectrocatalysts Prepared by Atomic Layer Deposition for Oxygen Evolution and Oxygen Reduction Reactions. Advanced Energy Materials. 2012;2:1269-77.

[57] Gorlin Y, Jaramillo TF. A bifunctional nonprecious metal catalyst for oxygen reduction and water oxidation. Journal of the American Chemical Society. 2010;132:13612-4.

[58] Gorlin Y, Nordlund D, Jaramillo TF. The Role of Heat Treatment in Enhanced Activity of Manganese Oxides for the Oxygen Reduction and Evolution Reactions. ECS Transactions. 2013;58:735-50.

[59] Selvakumar K, Kumar SS, Thangamuthu R, Kruthika G, Murugan P. Development of shape-engineered α-MnO 2 materials as bi-functional catalysts for oxygen evolution

reaction and oxygen reduction reaction in alkaline medium. International Journal of Hydrogen Energy. 2014;39:21024-36.

[60] Chen G, Yang H, Zhang H, Zhong H. Mn x Ir 1− x O 2/C used as bifunctional electrocatalyst in alkaline medium. Materials for Renewable Energy and Environment (ICMREE), 2013 International Conference on: IEEE; 2014. p. 440-4.

[61] Meng Y, Song W, Huang H, Ren Z, Chen S-Y, Suib SL. Structure–property relationship of bifunctional MnO2 nanostructures: highly efficient, ultra-stable electrochemical water oxidation and oxygen reduction reaction catalysts identified in alkaline media. Journal of the American Chemical Society. 2014;136:11452-64.

[62] Lin Z, Waller GH, Liu Y, Liu M, Wong C-p. Simple preparation of nanoporous few-layer nitrogen-doped graphene for use as an efficient electrocatalyst for oxygen reduction and oxygen evolution reactions. Carbon. 2013;53:130-6.

[63] Cheng Y, Tian Y, Fan X, Liu J, Yan C. Boron Doped Multi-walled Carbon Nanotubes as Catalysts for Oxygen Reduction Reaction and Oxygen Evolution Reactionin in Alkaline Media. Electrochimica Acta. 2014;143:291-6.

[64] Wang L, Yin F, Yao C. N-doped graphene as a bifunctional electrocatalyst for oxygen reduction and oxygen evolution reactions in an alkaline electrolyte. International Journal of Hydrogen Energy. 2014;39:15913-9.

[65] Zhang J, Zhao Z, Xia Z, Dai L. A metal-free bifunctional electrocatalyst for oxygen reduction and oxygen evolution reactions. Nature nanotechnology. 2015.

[66] Vineesh TV, Kumar MP, Takahashi C, Kalita G, Alwarappan S, Pattanayak DK, et al. Bifunctional Electrocatalytic Activity of Boron-Doped Graphene Derived from Boron Carbide. Advanced Energy Materials. 2015;5.

[67] Yadav RM, Wu J, Kochandra R, Ma L, Tiwary CS, Ge L, et al. Carbon Nitrogen Nanotubes as Efficient Bifunctional Electrocatalysts for Oxygen Reduction and Evolution Reactions. ACS applied materials & interfaces. 2015.

[68] Li B, Geng D, Lee XS, Ge X, Chai J, Wang Z, et al. Eggplant-derived microporous carbon sheets: towards mass production of efficient bifunctional oxygen electrocatalysts at low cost for rechargeable Zn–air batteries. Chemical Communications. 2015;51:8841-4.

[69] He D, Xiong Y, Yang J, Chen X, Deng Z, Pan M, et al. Nanocarbon-intercalated and Fe-N-codoped graphene as a highly active noble-metal-free bifunctional electrocatalyst for oxygen reduction and evolution. Journal of Materials Chemistry A. 2015.

[70] Yuan H, Deng L, Cai X, Zhou S, Chen Y, Yuan Y. Nitrogen-doped carbon sheets derived from chitin as non-metal bifunctional electrocatalysts for oxygen reduction and evolution. RSC Advances. 2015;5:56121-9.

[71] Lee KJ, Sa YJ, Jeong HY, Bielawski CW, Joo SH, Moon HR. Simple coordination complex-derived three-dimensional mesoporous graphene as an efficient bifunctional oxygen electrocatalyst. Chemical Communications. 2015;51:6773-6.

[72] Li R, Wei Z, Gou X. Nitrogen and Phosphorus Dual-doped Graphene/Carbon Nanosheets as Bifunctional Electrocatalysts for Oxygen Reduction and Evolution. ACS Catalysis. 2015.

[73] Hadidi L, Davari E, Iqbal M, Purkait TK, Ivey DG, Veinot JG. Spherical nitrogen-doped hollow mesoporous carbon as an efficient bifunctional electrocatalyst for Zn–air batteries. Nanoscale. 2015;7:20547-56.

[74] Qu K, Zheng Y, Dai S, Qiao SZ. Graphene oxide-polydopamine derived N, S-codoped carbon nanosheets as superior bifunctional electrocatalysts for oxygen reduction and evolution. Nano Energy. 2016;19:373-81.

[75] Yin F, Li G, Wang H. Hydrothermal synthesis of α-MnO 2/MIL-101 (Cr) composite and its bifunctional electrocatalytic activity for oxygen reduction/evolution reactions. Catalysis Communications. 2014;54:17-21.

[76] He X, Yin F, Li G. A Co/metal–organic-framework bifunctional electrocatalyst: The effect of the surface cobalt oxidation state on oxygen evolution/reduction reactions in an alkaline electrolyte. International Journal of Hydrogen Energy. 2015;40:9713-22.

[77] Wang H, Yin F, Li G, Chen B, Wang Z. Preparation, characterization and bifunctional catalytic properties of MOF (Fe/Co) catalyst for oxygen reduction/evolution reactions in alkaline electrolyte. International Journal of Hydrogen Energy. 2014;39:16179-86.

[78] Cao X, Yan W, Jin C, Tian J, Ke K, Yang R. Surface modification of MnCo 2 O 4 with conducting polypyrrole as a highly active bifunctional electrocatalyst for oxygen reduction and oxygen evolution reaction. Electrochimica Acta. 2015;180:788-94.

[79] Roy AL, Goenaga GA, Cantillo NM, Foister S, Zawodzinski TA. Novel Ni-Based Bifunctional Oxygen Catalysts for Metal Air Batteries and Alkaline Fuel Cells. Meeting Abstracts: The Electrochemical Society; 2015. p. 1566-.

[80] Sasikala N, Ramya K, Dhathathreyan KS. Bifunctional electrocatalyst for oxygen/air electrodes. Energy Conversion and Management. 2014;77:545-9.

[81] Yang Y, Fei H, Ruan G, Li L, Wang G, Kim ND, et al. Carbon-Free Electrocatalyst for Oxygen Reduction and Oxygen Evolution Reactions. ACS applied materials & interfaces. 2015;7:20607-11.

[82] Jin Y, Chen F. Facile preparation of Ag-Cu bifunctional electrocatalysts for zinc-air batteries. Electrochimica Acta. 2015;158:437-45.

[83] Liang Y, Li Y, Wang H, Zhou J, Wang J, Regier T, et al. Co3O4 nanocrystals on graphene as a synergistic catalyst for oxygen reduction reaction. Nature materials. 2011;10:780-6.

[84] Liu Y, Higgins DC, Wu J, Fowler M, Chen Z. Cubic spinel cobalt oxide/multi-walled carbon nanotube composites as an efficient bifunctionalelectrocatalyst for oxygen reaction. Electrochemistry Communications. 2013;34:125-9.

[85] Ma TY, Dai S, Jaroniec M, Qiao SZ. Metal–Organic Framework Derived Hybrid Co3O4-Carbon Porous Nanowire Arrays as Reversible Oxygen Evolution Electrodes. Journal of the American Chemical Society. 2014;136:13925-31.

[86] Masa J, Xia W, Sinev I, Zhao A, Sun Z, Grützke S, et al. MnxOy/NC and CoxOy/NC Nanoparticles Embedded in a Nitrogen-Doped Carbon Matrix for High-Performance Bifunctional Oxygen Electrodes. Angewandte Chemie International Edition. 2014;53:8508-12.

[87] Sun C, Li F, Ma C, Wang Y, Ren Y, Yang W, et al. Graphene–Co 3 O 4 nanocomposite as an efficient bifunctional catalyst for lithium–air batteries. Journal of Materials Chemistry A. 2014;2:7188-96.

[88] An T, Ge X, Hor TA, Goh FT, Geng D, Du G, et al. Co 3 O 4 nanoparticles grown on N-doped Vulcan carbon as a scalable bifunctional electrocatalyst for rechargeable zinc–air batteries. RSC Advances. 2015;5:75773-80.

[89] Andersen NI, Serov A, Atanassov P. Metal oxides/CNT nano-composite catalysts for oxygen reduction/oxygen evolution in alkaline media. Applied Catalysis B: Environmental. 2015;163:623-7.

[90] Li B, Ge X, Goh FT, Hor TA, Geng D, Du G, et al. Co 3 O 4 nanoparticles decorated carbon nanofiber mat as binder-free air-cathode for high performance rechargeable zinc-air batteries. Nanoscale. 2015;7:1830-8.

[91] Liu S, Li L, Ahn HS, Manthiram A. Delineating the roles of Co 3 O 4 and N-doped carbon nanoweb (CNW) in bifunctional Co 3 O 4/CNW catalysts for oxygen reduction and oxygen evolution reactions. Journal of Materials Chemistry A. 2015;3:11615-23.

[92] Lu X, Chan H, Sun C-L, Tseng C-M, Zhao C. Interconnected Core-Shell Carbon Nanotube/Graphene Nanoribbon Scaffolds for Anchorng Cobalt Oxides as Bifunctional Electrocatalysts for Oxygen Evolution and Reduction. Journal of Materials Chemistry A. 2015.

[93] Wang L, Zhao X, Lu Y, Xu M, Zhang D, Ruoff RS, et al. CoMn2O4 spinel nanoparticles grown on graphene as bifunctional catalyst for lithium-air batteries. Journal of The Electrochemical Society. 2011;158:A1379-A82.

[94] Prabu M, Ramakrishnan P, Nara H, Momma T, Osaka T, Shanmugam S. Zinc–Air Battery: Understanding the Structure and Morphology Changes of Graphene-Supported CoMn2O4 Bifunctional Catalysts Under Practical Rechargeable Conditions. ACS applied materials & interfaces. 2014;6:16545-55.

[95] Prabu M, Ramakrishnan P, Shanmugam S. CoMn2O4 nanoparticles anchored on nitrogen-doped graphene nanosheets as bifunctional electrocatalyst for rechargeable zinc–air battery. Electrochemistry Communications. 2014;41:59-63.

[96] Xu C, Lu M, Zhan Y, Lee JY. A bifunctional oxygen electrocatalyst from monodisperse MnCo 2 O 4 nanoparticles on nitrogen enriched carbon nanofibers. RSC Advances. 2014;4:25089-92.

[97] Zhao A, Masa J, Xia W, Maljusch A, Willinger M-G, Clavel G, et al. Spinel Mn–Co Oxide in N-Doped Carbon Nanotubes as a Bifunctional Electrocatalyst Synthesized by Oxidative Cutting. Journal of the American Chemical Society. 2014;136:7551-4.

[98] Kim JG, Kim Y, Noh Y, Kim WB. MnCo2O4 Nanowires Anchored on Reduced Graphene Oxide Sheets as Effective Bifunctional Catalysts for Li–O2 Battery Cathodes. ChemSusChem. 2015.

[99] Ge X. Spinel MnCo2O4 and Spinel-Nanocarbon Hybrids as Bifunctional Catalysts for Alternating Oxygen Reduction and Evolution Reactions. Materials for Energy Infrastructure: Springer; 2016. p. 83-91.

[100] Yan W, Bian W, Jin C, Tian J-H, Yang R. An Efficient Bi-functional Electrocatalyst Based on Strongly Coupled CoFe 2 O 4/Carbon Nanotubes Hybrid for Oxygen Reduction and Oxygen Evolution. Electrochimica Acta. 2015.

[101] Yan W, Yang Z, Bian W, Yang R. FeCo 2 O 4/hollow graphene spheres hybrid with enhanced electrocatalytic activities for oxygen reduction and oxygen evolution reaction. Carbon. 2015;92:74-83.

[102] Zhan Y, Xu C, Lu M, Liu Z, Lee JY. Mn and Co co-substituted Fe 3 O 4 nanoparticles on nitrogen-doped reduced graphene oxide for oxygen electrocatalysis in alkaline solution. Journal of Materials Chemistry A. 2014;2:16217-23.

[103] Yu X, Manthiram A. MnNiCoO 4/N-MWCNT nanocomposite catalyst with high selectivity in membraneless direct formate fuel cells and bifunctional activity for oxygen electrochemistry. Catalysis Science & Technology. 2015;5:2072-5.

[104] Chen Z, Yu A, Higgins D, Li H, Wang H, Chen Z. Highly active and durable core-corona structured bifunctional catalyst for rechargeable metal-air battery application. Nano Lett. 2012;12:1946-52.

[105] Hardin WG, Slanac DA, Wang X, Dai S, Johnston KP, Stevenson KJ. Highly active, nonprecious metal perovskite electrocatalysts for bifunctional metal–air battery electrodes. The Journal of Physical Chemistry Letters. 2013;4:1254-9.

[106] Lee DU, Park HW, Park MG, Ismayilov V, Chen Z. Synergistic Bifunctional Catalyst Design based on Perovskite Oxide Nanoparticles and Intertwined Carbon Nanotubes for Rechargeable Zinc–Air Battery Applications. ACS applied materials & interfaces. 2014;7:902-10.

[107] Xu Y, Tsou A, Fu Y, Wang J, Tian J-H, Yang R. Carbon-Coated Perovskite BaMnO 3 Porous Nanorods with Enhanced Electrocatalytic Perporites for Oxygen Reduction and Oxygen Evolution. Electrochimica Acta. 2015;174:551-6.

[108] Ge X, Goh FT, Li B, Hor TA, Zhang J, Xiao P, et al. Efficient and durable oxygen reduction and evolution of a hydrothermally synthesized La (Co 0.55 Mn 0.45) 0.99 O 3− δ nanorod/graphene hybrid in alkaline media. Nanoscale. 2015;7:9046-54.

[109] Lee DU, Park MG, Park HW, Seo MH, Ismayilov V, Ahmed R, et al. Highly active Co-doped LaMnO 3 perovskite oxide and N-doped carbon nanotube hybrid bi-functional catalyst for rechargeable zinc–air batteries. Electrochemistry Communications. 2015;60:38-41.

[110] Mohamed R, Fabbri E, Levecque P, Kötz R, Schmidt TJ, Conrad O. Understanding the Influence of Carbon on the Oxygen Reduction and Evolution Activities of BSCF/Carbon Composite Electrodes in Alkaline Electrolyte. Ecs Transactions. 2014;58:9-18.

[111] Zelenay P. (La, Sr) CoO 3-Rgo Hybrid Oxygen Reduction Reaction/Oxygen Evolution Reaction Bifunctional Catalyst. 227th ECS Meeting (May 24-28, 2015): Ecs; 2015.

[112] Park HW, Lee DU, Park MG, Ahmed R, Seo MH, Nazar LF, et al. Perovskite–Nitrogen-Doped Carbon Nanotube Composite as Bifunctional Catalysts for Rechargeable Lithium–Air Batteries. ChemSusChem. 2015;8:1058-65.

[113] Chen Z, Yu A, Ahmed R, Wang H, Li H, Chen Z. Manganese dioxide nanotube and nitrogen-doped carbon nanotube based composite bifunctional catalyst for rechargeable zinc-air battery. Electrochimica Acta. 2012;69:295-300.

[114] Gao Y, Zhao H, Chen D, Chen C, Ciucci F. In situ synthesis of mesoporous manganese oxide/sulfur-doped graphitized carbon as a bifunctional catalyst for oxygen evolution/reduction reactions. Carbon. 2015;94:1028-36.

[115] Ye D, Wu T, Cao H, Wang Y, Liu B, Zhang S, et al. Electrocatalysis of both oxygen reduction and water oxidation using a cost-effective three-dimensional MnO 2/graphene/carbon nanotube. RSC Advances. 2015;5:26710-5.

[116] Chen X, Botz AJ, Masa J, Schuhmann W. Characterisation of bifunctional electrocatalysts for oxygen reduction and evolution by means of SECM. J Solid State Electrochem. 2015:1-9.

[117] Mao S, Wen Z, Huang T, Hou Y, Chen J. High-performance bi-functional electrocatalysts of 3D crumpled graphene–cobalt oxide nanohybrids for oxygen reduction and evolution reactions. Energy & Environmental Science. 2014;7:609-16.

[118] Ganesan P, Prabu M, Sanetuntikul J, Shanmugam S. Cobalt Sulfide Nanoparticles Grown on Nitrogen and Sulfur Co-Doped Graphene Oxide: An Efficient Electrocatalyst for Oxygen Reduction and Evolution Reactions. ACS Catalysis. 2015.

[119] Geng D, Ding N-N, Hor TA, Chien SW, Liu Z, Zong Y. Cobalt sulfide nanoparticles impregnated nitrogen and sulfur co-doped graphene as bifunctional catalyst for rechargeable Zn–air batteries. RSC Advances. 2015;5:7280-4.

[120] Liu Q, Jin J, Zhang J. NiCo2S4@graphene as a Bifunctional Electrocatalyst for Oxygen Reduction and Evolution Reactions. ACS Applied Materials & Interfaces. 2013;5:5002-8.

[121] Shen M, Ruan C, Chen Y, Jiang C, Ai K, Lu L. Covalent Entrapment of Cobalt–Iron Sulfides in N-Doped Mesoporous Carbon: Extraordinary Bifunctional Electrocatalysts for Oxygen Reduction and Evolution Reactions. ACS applied materials & interfaces. 2015;7:1207-18.

[122] Liu X, Park M, Kim MG, Gupta S, Wu G, Cho J. Integrating NiCo Alloys with Their Oxides as Efficient Bifunctional Cathode Catalysts for Rechargeable Zinc–Air Batteries. Angewandte Chemie International Edition. 2015;54:9654-8.

[123] Phihusut D, Ocon JD, Jeong B, Kim JW, Lee JK, Lee J. Gently reduced graphene oxide incorporated into cobalt oxalate rods as bifunctional oxygen electrocatalyst. Electrochimica Acta. 2014;140:404-11.

[124] Garsuch A, Panchenko A, Querner C, Karpov A, Huber S, Oesten R. FeAgMo 2 O 8—A novel oxygen evolution catalyst material for alkaline metal–air batteries. Electrochemistry Communications. 2010;12:1642-5.

[125] Zhuang S, Huang K, Huang C, Huang H, Liu S, Fan M. Preparation of silver-modified La0.6Ca0.4CoO3 binary electrocatalyst for bi-functional air electrodes in alkaline medium. Journal of Power Sources. 2011;196:4019-25.

[126] Goh FT, Liu Z, Ge X, Zong Y, Du G, Hor TA. Ag nanoparticle-modified MnO 2 nanorods catalyst for use as an air electrode in zinc–air battery. Electrochimica Acta. 2013;114:598-604.

[127] Baltruschat H, Amin HM, Zan L, Ayata S, Soltani M. An Efficient Silver-Metal Oxide Hybrid Bifunctional Catalyst for Alkaline Air-Electrodes: DEMS and RRDE Study. Meeting Abstracts: The Electrochemical Society; 2014. p. 1529-.

[128] Amin HM, Baltruschat H, Wittmaier D, Friedrich KA. A Highly Efficient Bifunctional Catalyst for Alkaline Air-Electrodes Based on a Ag and Co 3 O 4 Hybrid: RRDE and Online DEMS Insights. Electrochimica Acta. 2015;151:332-9.

[129] Han X, Cheng F, Zhang T, Yang J, Hu Y, Chen J. Hydrogenated uniform Pt clusters supported on porous CaMnO3 as a bifunctional electrocatalyst for enhanced oxygen reduction and evolution. Advanced Materials. 2014;26:2047-51.

[130] Zhu Y, Su C, Xu X, Zhou W, Ran R, Shao Z. A Universal and Facile Way for the Development of Superior Bifunctional Electrocatalysts for Oxygen Reduction and

Evolution Reactions Utilizing the Synergistic Effect. Chemistry-A European Journal. 2014;20:15533-42.

[131] Hu S, Goenaga G, Melton C, Zawodzinski TA, Mukherjee D. PtCo/CoOx nanocomposites: Bifunctional electrocatalysts for oxygen reduction and evolution reactions synthesized via tandem laser ablation synthesis in solution-galvanic replacement reactions. Applied Catalysis B: Environmental. 2016;182:286-96.

[132] Rahaman H, Barman K, Jasimuddin S, Ghosh SK. Bifunctional gold–manganese oxide nanocomposites: benign electrocatalysts toward water oxidation and oxygen reduction. RSC Advances. 2014;4:41976-81.

[133] Du G, Liu X, Zong Y, Hor TA, Yu A, Liu Z. Co 3 O 4 nanoparticle-modified MnO 2 nanotube bifunctional oxygen cathode catalysts for rechargeable zinc–air batteries. Nanoscale. 2013;5:4657-61.

[134] Wang D, Chen X, Evans DG, Yang W. Well-dispersed Co3O4/Co2MnO4 nanocomposites as a synergistic bifunctional catalyst for oxygen reduction and oxygen evolution reactions. Nanoscale. 2013;5:5312-5.

[135] Risch M, Stoerzinger KA, Maruyama S, Hong WT, Takeuchi I, Shao-Horn Y. La0. 8Sr0. 2MnO3− δ Decorated with Ba0. 5Sr0. 5Co0. 8Fe0. 2O3− δ: A Bifunctional Surface for Oxygen Electrocatalysis with Enhanced Stability and Activity. Journal of the American Chemical Society. 2014;136:5229-32.

[136] Benhangi PH, Alfantazi A, Gyenge E. Manganese Dioxide-based Bifunctional Oxygen Reduction/Evolution Electrocatalysts: Effect of Perovskite Doping and Potassium Ion Insertion. Electrochimica Acta. 2014;123:42-50.

[137] Hosseini-Benhangi P, Garcia-Contreras MA, Alfantazi A, Gyenge EL. Method for Enhancing the Bifunctional Activity and Durability of Oxygen Electrodes with Mixed Oxide Electrocatalysts: Potential Driven Intercalation of Potassium. Journal of The Electrochemical Society. 2015;162:F1356-F66.

[138] Su Y, Zhu Y, Jiang H, Shen J, Yang X, Zou W, et al. Cobalt nanoparticles embedded in N-doped carbon as an efficient bifunctional electrocatalyst for oxygen reduction and evolution reactions. Nanoscale. 2014;6:15080-9.

[139] Singhal R, Kalra V. Cobalt Nanoparticles Embedded in Porous Carbon Nanofibers As Bifunctional Electrocatalysts for Oxygen Reduction and Evolution Reactions. Meeting Abstracts: The Electrochemical Society; 2015. p. 28-.

[140] Wang Z, Xiao S, Zhu Z, Long X, Zheng X, Lu X, et al. Cobalt-Embedded Nitrogen Doped Carbon Nanotubes: A Bifunctional Catalyst for Oxygen Electrode Reactions in a Wide pH Range. ACS applied materials & interfaces. 2015;7:4048-55.

[141] Zhao Y, Kamiya K, Hashimoto K, Nakanishi S. Efficient Bifunctional Fe/C/N Electrocatalysts for Oxygen Reduction and Evolution Reaction. The Journal of Physical Chemistry C. 2015;119:2583-8.

[142] Liu Y, Jiang H, Zhu Y, Yang X, Li C. Transitional Metal (Fe, Co, Ni) Encapsulated in Nitrogen-Doped Carbon Nanotubes as Bi-functional Catalysts for Oxygen Electrode Reactions. Journal of Materials Chemistry A. 2016.

[143] Wu Y, Zang J, Dong L, Zhang Y, Wang Y. High performance and bifunctional cobalt-embedded nitrogen doped carbon/nanodiamond electrocatalysts for oxygen reduction and oxygen evolution reactions in alkaline media. Journal of Power Sources. 2016;305:64-71.

[144] Li X, Pletcher D, Russell AE, Walsh FC, Wills RGA, Gorman SF, et al. A novel bifunctional oxygen GDE for alkaline secondary batteries. Electrochemistry Communications. 2013;34:228-30.

[145] Price SWT, Thompson SJ, Li X, Gorman SF, Pletcher D, Russell AE, et al. The fabrication of a bifunctional oxygen electrode without carbon components for alkaline secondary batteries. Journal of Power Sources. 2014;259:43-9.

[146] Silva RA, Soares CO, Carvalho MD, Rangel CM, da Silva Pereira MI. Stability of LaNiO3 gas diffusion oxygen electrodes. J Solid State Electrochem. 2014;18:821-31.

[147] Wittmaier D, Aisenbrey S, Wagner N, Friedrich KA. Bifunctional, Carbon-Free Nickel/Cobalt-Oxide Cathodes for Lithium-Air Batteries with an Aqueous Alkaline Electrolyte. Electrochimica Acta. 2014;149:355-63.

[148] Pletcher D, Li X, Price SW, Russell AE, Sönmez T, Thompson SJ. Comparison of the Spinels Co 3 O 4 and NiCo 2 O 4 as Bifunctional Oxygen Catalysts in Alkaline Media. Electrochimica Acta. 2016;188:286-93.

[149] Desmond Ng JW, Gorlin Y, Hatsukade T, Jaramillo TF. A Precious-Metal-Free Regenerative Fuel Cell for Storing Renewable Electricity. Advanced Energy Materials. 2013;3:1545-50.

[150] Bretthauer C, Müller C, Reinecke H. Design and fabrication of a MEMS-based metal hydride/air accumulator for energy harvesting. Electrochimica Acta. 2009;54:6094-8.

[151] Bretthauer C, Müller C, Reinecke H. A precious-metal free micro fuel cell accumulator. Journal of Power Sources. 2011;196:4729-34.

[152] Laguna-Bercero MA, Kinadjan N, Sayers R, El Shinawi H, Greaves C, Skinner SJ. Performance of La2-xSrxCo0.5Ni0.5O4±δ as an Oxygen Electrode for Solid Oxide Reversible Cells. Fuel Cells. 2011;11:102-7.

[153] Laguna-Bercero MA, Campana R, Larrea A, Kilner JA, Orera VM. Performance and Aging of Microtubular YSZ-based Solid Oxide Regenerative Fuel Cells. Fuel Cells. 2011;11:116-23.

[154] Ni M, Leung M, Leung D. Technological development of hydrogen production by solid oxide electrolyzer cell (SOEC). International Journal of Hydrogen Energy. 2008;33:2337-54.

[155] Ruiz-Morales JC, Marrero-López D, Canales-Vázquez J, Irvine JTS. Symmetric and reversible solid oxide fuel cells. RSC Advances. 2011;1:1403.

[156] Laguna-Bercero MA. Recent advances in high temperature electrolysis using solid oxide fuel cells: A review. Journal of Power Sources. 2012;203:4-16.

[157] Moçoteguy P, Brisse A. A review and comprehensive analysis of degradation mechanisms of solid oxide electrolysis cells. International Journal of Hydrogen Energy. 2013;38:15887-902.

[158] Bi L, Boulfrad S, Traversa E. Reversible solid oxide fuel cells (R-SOFCs) with chemically stable proton-conducting oxides. Solid State Ionics. 2015;275:101-5.

[159] Brisse A, Schefold J, Zahid M. High temperature water electrolysis in solid oxide cells. International Journal of Hydrogen Energy. 2008;33:5375-82.

[160] Lee S-i, Kim J, Son J-W, Lee J-H, Kim B-K, Je H-J, et al. High performance air electrode for solid oxide regenerative fuel cells fabricated by infiltration of nano-catalysts. Journal of Power Sources. 2014;250:15-20.

[161] Erdle E, Dönitz W, Schamm R, Koch A. Reversibility and polarization behaviour of high temperature solid oxide electrochemical cells. International journal of hydrogen energy. 1992;17:817-9.

[162] Shimaki R, Okamoto M, Yanagi C, Kikuoka Y, Ueda S, Nakamori N, et al. Feasibility study on hydrogen-utilized electric power storage systems. Hydrogen energy progress IX Volume 31993.

[163] Kusunoki D, Kikuoka Y, Yanagi V, Kugimiya K, Yoshino M, Tokura M, et al. Development of Mitsubishi-planar reversible cell—Fundamental test on hydrogen-utilized electric power storage system. International journal of hydrogen energy. 1995;20:831-4.

[164] Minh NQ, Mogensen MB. Reversible solid oxide fuel cell technology for green fuel and power production. Electrochem Soc Interface. 2013;22:55-62.

[165] Eguchi K, Hatagishi T, Arai H. Power generation and steam electrolysis characteristics of an electrochemical cell with a zirconia- or ceria-based electrolyte. Solid State Ionics. 1996;86–88, Part 2:1245-9.

[166] Momma A, Kato T, Kaga Y, Nagata S. Polarization behavior of high temperature solid oxide electrolysis cells (SOEC). Nippon seramikkusu kyokai gakujutsu ronbunshi. 1997;105:369-73.

[167] Matsui T, Ozaki A, Kikuchi R, Eguchi K. Influence of steam concentration on the degradation behavior of reversible solid oxide fuel cells. Proceedings-Electrochemical Society: Electrochemical Society; 2005.

[168] Uchida H, Osada N, Suzuki S, Watanabe M. High performance electrodes for reversible solid oxide fuel cells. Proceedings-Electrochemical Society: Electrochemical Society; 2005.

[169] Bastidas DM, Tao S, Irvine JTS. A symmetrical solid oxide fuel cell demonstrating redox stable perovskite electrodes. Journal of Materials Chemistry. 2006;16:1603.

[170] Gopalan S, Ye G, Pal UB. Regenerative, coal-based solid oxide fuel cell-electrolyzers. Journal of Power Sources. 2006;162:74-80.

[171] McElroy JF, Hickey DB, Mitlitsky F. Optimization and Demonstration of a Solid Oxide Regenerative Fuel Cell System. Ion America Corporation; 2006.

[172] Elangovan S, Hartvigsen JJ, Frost LJ. Intermediate temperature reversible fuel cells. International journal of applied ceramic technology. 2007;4:109-18.

[173] Marina OA, Pederson LR, Williams MC, Coffey GW, Meinhardt KD, Nguyen CD, et al. Electrode Performance in Reversible Solid Oxide Fuel Cells. Journal of The Electrochemical Society. 2007;154:B452.

[174] Hauch A, Ebbesen SD, Jensen SH, Mogensen M. Solid Oxide Electrolysis Cells: Microstructure and Degradation of the Ni/Yttria-Stabilized Zirconia Electrode. Journal of The Electrochemical Society. 2008;155:B1184.

[175] Schiller G, Ansar A, Lang M, Patz O. High temperature water electrolysis using metal supported solid oxide electrolyser cells (SOEC). Journal of Applied Electrochemistry. 2008;39:293-301.

[176] Tao Y, Nishino H, Ashidate S, Kokubo H, Watanabe M, Uchida H. Polarization properties of La0.6Sr0.4Co0.2Fe0.8O3-based double layer-type oxygen electrodes for reversible SOFCs. Electrochimica Acta. 2009;54:3309-15.

[177] Zhan Z, Kobsiriphat W, Wilson JR, Pillai M, Kim I, Barnett SA. Syngas production by coelectrolysis of CO2/H2O: the basis for a renewable energy cycle. Energy & Fuels. 2009;23:3089-96.

[178] Zhan Z, Zhao L. Electrochemical reduction of CO2 in solid oxide electrolysis cells. Journal of Power Sources. 2010;195:7250-4.

[179] Cable TL, Setlock JA, Farmer SC, Eckel AJ. Regenerative Performance of the NASA Symmetrical Solid Oxide Fuel Cell Design. International Journal of Applied Ceramic Technology. 2011;8:1-12.

[180] Kim-Lohsoontorn P, Bae J. Electrochemical performance of solid oxide electrolysis cell electrodes under high-temperature coelectrolysis of steam and carbon dioxide. Journal of Power Sources. 2011;196:7161-8.

[181] Laguna-Bercero MA, Kilner JA, Skinner SJ. Development of oxygen electrodes for reversible solid oxide fuel cells with scandia stabilized zirconia electrolytes. Solid State Ionics. 2011;192:501-4.

[182] Moyer CJ, Sullivan NP, Zhu H, Kee RJ. Polarization Characteristics and Chemistry in Reversible Tubular Solid-Oxide Cells Operating on Mixtures of H[sub 2], CO, H[sub 2]O, and CO[sub 2]. Journal of The Electrochemical Society. 2011;158:B117.

[183] Jung G-B, Chen J-Y, Lin C-Y, Sun S-Y. Fabrication of hydrogen electrode supported cell for utilized regenerative solid oxide fuel cell application. International Journal of Hydrogen Energy. 2012;37:15801-7.

[184] Rao Y, Wang Z, Zhong W, Peng R, Lu Y. Novel Ni–Ba1+xZr0.3Ce0.5Y0.2O3−δ hydrogen electrodes as effective reduction barriers for reversible solid oxide cells based on doped ceria electrolyte thin film. Journal of Power Sources. 2012;199:142-5.

[185] Choi M-B, Singh B, Wachsman ED, Song S-J. Performance of La0.1Sr0.9Co0.8Fe0.2O3−δ and La0.1Sr0.9Co0.8Fe0.2O3−δ–Ce0.9Gd0.1O2 oxygen electrodes with Ce0.9Gd0.1O2 barrier layer in reversible solid oxide fuel cells. Journal of Power Sources. 2013;239:361-73.

[186] Nguyen VN, Fang Q, Packbier U, Blum L. Long-term tests of a Jülich planar short stack with reversible solid oxide cells in both fuel cell and electrolysis modes. International Journal of Hydrogen Energy. 2013;38:4281-90.

[187] Su Q, Yoon D, Sisman Z, Khatkhatay F, Jia Q, Manthiram A, et al. Vertically aligned nanocomposite La0.8Sr0.2MnO3−δ/Zr0.92Y0.08O1.96 thin films as electrode/electrolyte interfacial layer for solid oxide reversible fuel cells. International Journal of Hydrogen Energy. 2013;38:16320-7.

[188] Fan H, Keane M, Li N, Tang D, Singh P, Han M. Electrochemical stability of La0.6Sr0.4Co0.2Fe0.8O3−δ-infiltrated YSZ oxygen electrode for reversible solid oxide fuel cells. International Journal of Hydrogen Energy. 2014;39:14071-8.

[189] Fan H, Keane M, Singh P, Han M. Electrochemical performance and stability of lanthanum strontium cobalt ferrite oxygen electrode with gadolinia doped ceria barrier layer for reversible solid oxide fuel cell. Journal of Power Sources. 2014;268:634-9.

[190] Hong J, Kim H-J, Park S-Y, Lee J-H, Park S-B, Lee J-H, et al. Electrochemical performance and long-term durability of a 200 W-class solid oxide regenerative fuel cell stack. International Journal of Hydrogen Energy. 2014;39:20819-28.

[191] Yoon KJ, Lee S-i, An H, Kim J, Son J-W, Lee J-H, et al. Gas transport in hydrogen electrode of solid oxide regenerative fuel cells for power generation and hydrogen production. International Journal of Hydrogen Energy. 2014;39:3868-78.

[192] Chen T, Zhou Y, Liu M, Yuan C, Ye X, Zhan Z, et al. High performance solid oxide electrolysis cell with impregnated electrodes. Electrochemistry Communications. 2015;54:23-7.

[193] Ferrero D, Lanzini A, Leone P, Santarelli M. Reversible operation of solid oxide cells under electrolysis and fuel cell modes: Experimental study and model validation. Chemical Engineering Journal. 2015;274:143-55.

[194] Molero-Sánchez B, Prado-Gonjal J, Ávila-Brande D, Chen M, Morán E, Birss V. High performance La0.3Ca0.7Cr0.3Fe0.7O3−δ air electrode for reversible solid oxide fuel cell applications. International Journal of Hydrogen Energy. 2015;40:1902-10.

[195] Yoo Y-S, Choi M, Hwang J-H, Im H-N, Singh B, Song S-J. La2NiO4+δ as oxygen electrode in reversible solid oxide cells. Ceramics International. 2015;41:6448-54.

[196] Stuart PA, Unno T, Kilner JA, Skinner SJ. Solid oxide proton conducting steam electrolysers. Solid State Ionics. 2008;179:1120-4.

[197] He F, Song D, Peng R, Meng G, Yang S. Electrode performance and analysis of reversible solid oxide fuel cells with proton conducting electrolyte of BaCe0.5Zr0.3Y0.2O3−δ. Journal of Power Sources. 2010;195:3359-64.

[198] Azimova MA, McIntosh S. On the reversibility of anode supported proton conducting solid oxide cells. Solid State Ionics. 2011;203:57-61.

[199] Rao Y, Zhong S, He F, Wang Z, Peng R, Lu Y. Cobalt-doped BaZrO3: A single phase air electrode material for reversible solid oxide cells. International Journal of Hydrogen Energy. 2012;37:12522-7.

[200] Yoo Y, Lim N. Performance and stability of proton conducting solid oxide fuel cells based on yttrium-doped barium cerate-zirconate thin-film electrolyte. Journal of Power Sources. 2013;229:48-57.

[201] Viviani M, Canu G, Carpanese MP, Barbucci A, Sanson A, Mercadelli E, et al. Dual Cells with Mixed Protonic-Anionic Conductivity for Reversible SOFC/SOEC Operation. Energy Procedia. 2012;28:182-9.

[202] Zheng K-Q, Ni M, Sun Q, Shen L-Y. Mathematical analysis of SOFC based on co-ionic conducting electrolyte. Acta mechanica sinica. 2013;29:388-94.

[203] Ni M, Leung MKH, Leung DYC. Micro-scale modelling of solid oxide fuel cells with micro-structurally graded electrodes. Journal of Power Sources. 2007;168:369-78.

[204] Yokokawa H, Tu H, Iwanschitz B, Mai A. Fundamental mechanisms limiting solid oxide fuel cell durability. Journal of Power Sources. 2008;182:400-12.

[205] Zhang Y, Chen K, Xia C, Jiang SP, Ni M. A model for the delamination kinetics of La 0.8 Sr 0.2 MnO 3 oxygen electrodes of solid oxide electrolysis cells. International journal of hydrogen energy. 2012;37:13914-20.

[206] Liu Q, Dong X, Xiao G, Zhao F, Chen F. A Novel Electrode Material for Symmetrical SOFCs. Advanced Materials. 2010;22:5478-82.

[207] Liu Q, Yang C, Dong X, Chen F. Perovskite Sr2Fe1.5Mo0.5O6−δ as electrode materials for symmetrical solid oxide electrolysis cells. International Journal of Hydrogen Energy. 2010;35:10039-44.

[208] Ni M. 2D thermal modeling of a solid oxide electrolyzer cell (SOEC) for syngas production by H 2 O/CO 2 co-electrolysis. International journal of hydrogen energy. 2012;37:6389-99.

[209] Ni M. An electrochemical model for syngas production by co-electrolysis of H 2 O and CO 2. Journal of power sources. 2012;202:209-16.

[210] Ni M, Leung MKH, Leung DYC. Mathematical Modelling of Proton-Conducting Solid Oxide Fuel Cells and Comparison with Oxygen-Ion-Conducting Counterpart. Fuel Cells. 2007;7:269-78.

[211] Iwahara H, Esaka T, Uchida H, Maeda N. Proton conduction in sintered oxides and its application to steam electrolysis for hydrogen production. Solid State Ionics. 1981;3–4:359-63.

[212] Jin X, Xue X. Mathematical modeling analysis of regenerative solid oxide fuel cells in switching mode conditions. Journal of Power Sources. 2010;195:6652-8.

[213] Ni M, Leung MKH, Leung DYC. A modeling study on concentration overpotentials of a reversible solid oxide fuel cell. Journal of Power Sources. 2006;163:460-6.

[214] Ni M, Leung MKH, Leung DYC. Theoretical analysis of reversible solid oxide fuel cell based on proton-conducting electrolyte. Journal of Power Sources. 2008;177:369-75.

[215] Ni M, Leung MKH, Leung DYC. Electrochemical modeling of hydrogen production by proton-conducting solid oxide steam electrolyzer. International Journal of Hydrogen Energy. 2008;33:4040-7.

[216] Su A, Ferng YM, Wang CB, Cheng CH. Analytically investigating the characteristics of a high-temperature unitized regenerative solid oxide fuel cell. International Journal of Energy Research. 2013;37:1699-708.

[217] Su A, Ferng YM, Wang C. Investigating parametric effects on performance of a high-temperature URSOFC. International Journal of Energy Research. 2015;39:648-60.

[218] García-Camprubí M, Izquierdo S, Fueyo N. Challenges in the electrochemical modelling of solid oxide fuel and electrolyser cells. Renewable and Sustainable Energy Reviews. 2014;33:701-18.

[219] Kazempoor P, Braun RJ. Model validation and performance analysis of regenerative solid oxide cells for energy storage applications: Reversible operation. International Journal of Hydrogen Energy. 2014;39:5955-71.

[220] Wendel CH, Gao Z, Barnett SA, Braun RJ. Modeling and experimental performance of an intermediate temperature reversible solid oxide cell for high-efficiency, distributed-scale electrical energy storage. Journal of Power Sources. 2015;283:329-42.

[221] Wendel CH, Kazempoor P, Braun RJ. Novel electrical energy storage system based on reversible solid oxide cells: System design and operating conditions. Journal of Power Sources. 2015;276:133-44.

[222] Ren J, Gamble SR, Roscoe AJ, Irvine JTS, Burt G. Modeling a Reversible Solid Oxide Fuel Cell as a Storage Device Within AC Power Networks. Fuel Cells. 2012;12:773-86.

[223] Ferrigno R, Stroock AD, Clark TD, Mayer M, Whitesides GM. Membraneless vanadium redox fuel cell using laminar flow. Journal of the American Chemical Society. 2002;124:12930-1.

[224] Kjeang E, McKechnie J, Sinton D, Djilali N. Planar and three-dimensional microfluidic fuel cell architectures based on graphite rod electrodes. Journal of Power Sources. 2007;168:379-90.

[225] Kjeang E, Proctor BT, Brolo AG, Harrington DA, Djilali N, Sinton D. High-performance microfluidic vanadium redox fuel cell. Electrochimica Acta. 2007;52:4942-6.

[226] Kjeang E, Michel R, Harrington DA, Djilali N, Sinton D. A microfluidic fuel cell with flow-through porous electrodes. Journal of the American Chemical Society. 2008;130:4000-6.

[227] Jayashree RS, Mitchell M, Natarajan D, Markoski LJ, Kenis PJ. Microfluidic hydrogen fuel cell with a liquid electrolyte. Langmuir. 2007;23:6871-4.

[228] Brushett FR, Zhou W-P, Jayashree RS, Kenis PJA. Alkaline Microfluidic Hydrogen-Oxygen Fuel Cell as a Cathode Characterization Platform. Journal of The Electrochemical Society. 2009;156:B565.

[229] Choban ER, Waszczuk P, Kenis PJA. Characterization of Limiting Factors in Laminar Flow-Based Membraneless Microfuel Cells. Electrochemical and Solid-State Letters. 2005;8:A348.

[230] Brushett FR, Jayashree RS, Zhou W-P, Kenis PJA. Investigation of fuel and media flexible laminar flow-based fuel cells. Electrochimica Acta. 2009;54:7099-105.

[231] Choban E. Microfluidic fuel cell based on laminar flow. Journal of Power Sources. 2004;128:54-60.

[232] Cohen JL, Westly DA, Pechenik A, Abruña HD. Fabrication and preliminary testing of a planar membraneless microchannel fuel cell. Journal of Power Sources. 2005;139:96-105.

[233] Zhang H, Xuan J, Xu H, Leung MKH, Leung DYC, Zhang L, et al. Enabling high-concentrated fuel operation of fuel cells with microfluidic principles: A feasibility study. Applied Energy. 2013;112:1131-7.

[234] Xuan J, Leung MKH, Leung DYC, Ni M, Wang H. Hydrodynamic focusing in microfluidic membraneless fuel cells: Breaking the trade-off between fuel utilization and current density. International Journal of Hydrogen Energy. 2011;36:11075-84.

[235] Wang Y, Leung DY, Xuan J, Wang H. A vapor feed methanol microfluidic fuel cell with high fuel and energy efficiency. Applied Energy. 2015;147:456-65.

[236] Salloum KS, Posner JD. A membraneless microfluidic fuel cell stack. Journal of Power Sources. 2011;196:1229-34.

[237] Wang H, Gu S, Leung DYC, Xu H, Leung MKH, Zhang L, et al. Development and characteristics of a membraneless microfluidic fuel cell array. Electrochimica Acta. 2014;135:467-77.

[238] Zhang H, Leung MKH, Xuan J, Xu H, Zhang L, Leung DYC, et al. Energy and exergy analysis of microfluidic fuel cell. International Journal of Hydrogen Energy. 2013;38:6526-36.

[239] Wang H, Leung DYC, Xuan J. Modeling of an air cathode for microfluidic fuel cells: Transport and polarization behaviors. International Journal of Hydrogen Energy. 2011;36:14704-18.

[240] Xuan J, Leung MKH, Leung DYC, Ni M. Density-induced asymmetric pair of Dean vortices and its effects on mass transfer in a curved microchannel with two-layer laminar stream. Chemical Engineering Journal. 2011;171:216-23.

[241] Xuan J, Leung MKH, Leung DYC, Wang H. Laminar flow-based fuel cell working under critical conditions: The effect of parasitic current. Applied Energy. 2012;90:87-93.

[242] Xuan J, Leung MKH, Leung DYC, Wang H. Towards orientation-independent performance of membraneless microfluidic fuel cell: Understanding the gravity effects. Applied Energy. 2012;90:80-6.

[243] Xuan J, Leung DYC, Wang H, Leung MKH, Wang B, Ni M. Air-breathing membraneless laminar flow-based fuel cells: Do they breathe enough oxygen? Applied Energy. 2013;104:400-7.

[244] Xuan J, Wang H, Leung DYC, Leung MKH, Xu H, Zhang L, et al. Theoretical Graetz–Damköhler modeling of an air-breathing microfluidic fuel cell. Journal of Power Sources. 2013;231:1-5.

[245] Lu X, Leung, D.Y.C., Wang, H.Z., Leung, M.K.H., Xuan, J. Microfluidic Reversible Fuel Cell for Carbon-Neutral Energy Conversion Cycle. Compendium on Energy Science and Technology: Studium Press LLC, USA.

[246] Whipple DT, Finke EC, Kenis PJ. Microfluidic reactor for the electrochemical reduction of carbon dioxide: the effect of pH. Electrochemical and Solid-State Letters. 2010;13:B109-B11.

[247] Xuan J, Leung DYC, Leung MKH, Ni M, Wang H. A computational study of bifunctional oxygen electrode in air-breathing reversible microfluidic fuel cells. International Journal of Hydrogen Energy. 2011;36:9231-41.

[248] Wang H, Leung DYC, Xuan J. Modeling of a microfluidic electrochemical cell for CO2 utilization and fuel production. Applied Energy. 2013;102:1057-62.

**Figure captions:**

**Fig.1** SEM images of various hybrid BOCs with synergistic effects: (a) $Co_3O_4$/N-rmGO [83]; (b) Ag modified $La_{0.6}Ca_{0.4}CoO_3$ [125]; (c) Core−corona structured $LaNiO_3$-NCNTs [104]; (d) $NiCo_2S_4$@N/S-rGO [120]; (e) B-MWCNTs [63]; (f) $CoMn_2O_4$/N-rGO [95]; (g) $CoC_2O_4$/gRGO [123]

**Fig.2** Evidence of the carbon-based electrode corrosion in alkaline environment [146]: (a) before 200 cycles; (b) after 200 cycles

**Fig.3** A UR-AFC based on the RP-$LaSr_3Fe_3O_{10}$ oxygen electrode shows much lower overpotentials in both modes [16]: (a) cell composition; (b) polarization curve

**Fig.4** Calculated energy demand for water electrolysis under various temperatures [154]

**Fig.5** Schematic diagram of different hydrogen electrode structures [158]: (a) conventional one-layer structure; (b) Two-layer structure

**Fig.6** A novel BHE with Ni particles dispersed in porous YSZ scaffold, which alleviate the Ni agglomeration problem after EC mode operation [179]

**Fig.7** Major degradation mechanisms to a single RSOFC: (a) Ni particle agglomeration [204]; (b) Si-containing impurities (red) from glass sealants [174]; (c) oxygen electrode delamination [190]; (d) YSZ electrolyte reduction [153]

**Fig.8** Stability study of various RSOFCs in regenerative mode operation: (a) From Hong et al. [190] (b)(c) From Fan et al. [188, 189] (d)(e) From McElroy et al. [171]

**Fig.9** RSOFC-O stack prototypes in the literature: (a) NASA all-ceramic stack by Cable et al. [179] (b) Jülich 2-cell stack by Nguyen et al. [186] (c) 200W-class 3-cell stack by Hong et al. [190]

**Fig.10** Micro-tubular RSOFC prototype [182]

**Fig.11** Schematic diagram of RSOFCs with syngas operation

**Fig.12** I-V characteristics of single cells prepared by different fabrication processes and electrolyte materials at 600℃ under humid 75% $H_2$ in Ar (2.76% $H_2O$) and humid air [200]

**Fig.13** Microfluidic fuel cells with various structures [9]: (a) T-type with electrodes on the channel bottom; (b) T-type with electrodes on the channel sides; (c) F-type air-breathing cathode; (d) Flow-through electrodes

**Fig.14** Schematic diagram of an air-breathing RMFC [247]: (a) FC mode; (b) EC mode

**Tables:**

**Table-1** AEM-based UR-AFC prototypes demonstrated to date

| **References** | **BHC** | **Electrolyte** | **BOC** | **GDL** | **Temp. (℃)** | **PPD (mWcm$^{-2}$)** | **RT-efficiency** | **Stability** |
|---|---|---|---|---|---|---|---|---|
| Wu et al. [15] | 50wt.% Pt/C (1mg$_{Pt}$cm$^{-2}$) | Homemade AEM | $Cu_{0.6}Mn_{0.3}Co_{2.1}O_4$ (3mgcm$^{-2}$) | Carbon paper (BHE&BOE) | 40 | 80 | 31.9% at 100mAcm$^{-2}$ | |
| Wu et al. [18] | 20wt.% Pt/C (0.1mgcm$^{-2}$) | Porous PTFE filled with qPDTB-OH$^-$ | $Cu_{0.6}Mn_{0.3}Co_{2.1}O_4$ | Au-coated Ti mesh (BOE) | 20, 45 | 114 (20℃) 163 (45℃) | 34% at 100mAcm$^{-2}$ (22℃) | Degradation rate of 0.0379mVh$^{-1}$ at 100mAcm$^{-2}$ in EC mode for the first 120hrs (22℃). |
| Ng et al. [149] | Ni/C (6mgcm$^{-2}$) | AEM (FAA-3,Fumatech) | Ni/C + $MnO_x$/GC (1:5 by mass, 4mgcm$^{-2}$) | Carbon paper (BOE) | 65 | 16.5 | 40% at 10mAcm$^{-2}$ | RT-efficiency dropped from 40% to 34% after 8 cycles (160mins) |
| Ng et al. [17] | 46wt.% Pt/C 0.5mgcm$^{-2}$ | AEM (FAA-3-PK-130, Fumatech) | $MnO_x$ (0.3mgcm$^{-2}$) | Carbon paper (BHE) Stainless steel (BOE) | 55 | 27 | 42-45% at 20mAcm$^{-2}$ | Quite stable for 10 cycles, with RT-efficiency dropped from 45% to 42%. |
| Takeguchi et al. [16] | 46.5wt.% Pt/C 0.5mgcm$^{-2}$ | AEM (A201, Tokuyama) | RP-$LaSr_3Fe_3O_{10}$ pellet (1mm thickness) | Carbon paper (BHE) | 60 | | | |
| Bretthauer et al. [150] | $LaNi_5$ MH | AEM (Tokuyama) | Pt | | | 0.559 | | |
| Bretthauer et al. [151] | $LaNi_5$ MH | AEM (A3PE, Tokuyama) | $La_{0.6}Ca_{0.4}CoO_3$/C | | | 0.66 | 52% at 0.1mAcm$^{-2}$ 23% at 0.31V | Very stable in WE mode at 1mAcm$^{-2}$ and in FC mode at 0.5-2mAcm$^{-2}$ |

**Table-2** RSOFC-O prototypes demonstrated to date

| References | BHE | Electrolyte | BOE | Temp. (℃) | PPD ($mWcm^{-2}$) | Stability |
|---|---|---|---|---|---|---|
| Kusunoki et al. [163] | Ni-YSZ | 8YSZ (500µm) | LSM | 1000 | | |
| Eguchi et al. [165] | Ni-YSZ; Pt | YSZ (500µm) + SDC (2µm) | LSM; LSC | 1000 | | |
| Momma et al. [166] | Ni-YSZ | YSZ (0.5-1mm) + SDC | LSM; LSC; LC | 1000 | | Oxygen electrode delamination from the electrolyte after long-term electrolysis operation |
| Uchida et al. [168] | Ni/SDC | 8YSZ (1mm) + SDC (1µm) | LSC; LSCF; Pt | 800 (FC mode) 900 (WE mode) | | Stable performance of the Ni/SDC anode at 800℃ and $0.6Acm^{-2}$ for over 1100hrs |
| Matsui et al. [167] | Ni-YSZ | 8YSZ (0.5mm) | LSM | 1000 | | Unstable under limited fuel condition in FC mode and limited $H_2O$ condition in WE mode |
| Bastidas et al. [b] [169] | LSCM-YSZ + LSCMx2 (50µm) | YSZ (0.2mm) | LSCM-YSZ + LSCMx2 (50µm) | 900 | 300 | Stable in half-cell test for 4 cycles in both hydrogen and oxygen atmosphere |
| McElroy et al. [171] | Ni-electrolyte material | YSZ (300µm) | LSM; LSC; LCC; LSCF etc. | 850 | | Very good stability in regenerative mode: degradation rate of the RT efficiency can be as low as 0.5%/1000h in regenerative mode |
| Gopalan et al. [170] | Ni-YSZ | YSZ | Liquid Ag | 1000 | | |
| Marina et al. [173] | Ni-YSZ + Ni-YSZ (550µm) | YSZ (7µm) + SDC (2µm) | LSCF (30µm) | 750 | | |
| Elangovan et al. [c] [172] | Ni(MgO)-$CeO_2$ | LSGM | LSC | 700-800 | | |
| Hauch et al. [174] | Ni-YSZ (10-15µm) + Ni-YSZ (~300µm) | YSZ (10-15µm) | LSM-YSZ (15-20µm) | 850 | | Voltage degradation of 2%/1000h was obtained in WE |

| | | | | | | |
|---|---|---|---|---|---|---|
| | | | | | | mode at 0.5Acm$^{-2}$ |
| Schiller et al. [175] | Ni-YSZ (~50µm) +metal support | YSZ (~40µm) | LSCF (~30µm) | 750-850 | | Degradation rate of 3.2%/1000h in EC mode at 0.3Acm$^{-2}$ for 2000hrs |
| Tao et al. [176] | Pt | YSZ (1mm) + SDC (1µm) | LSCF-SDC (30µm) + LSCF (10µm) | 700-900 | | |
| Zhan et al. [177] | Ni-YSZ + Ni-YSZ (~600µm) | YSZ (~10µm) | LSCF-GDC+LSCF (20-30µm) | 700-800 | | Voltage increased by ~2% during 100h electrolysis at 1.05Acm$^{-2}$ |
| Liu et al. [b] [206, 207] | SFM (70 µm) | LSGM (320 µm) | SFM (70 µm) | 800-900 | 835 (900℃) | Stable performance in EC mode at 1.2V for 100hrs |
| Zhan et al. [178] | Ni-YSZ (20µm) + Ni-YSZ (600µm) | YSZ (15µm) | LSCF-GDC (30µm) + LSCF | 700-800 | | |
| Bercero et al. [181] | Ni-YSZ (5µm) + Ni-YSZ (25-30µm) | 10Sc1CeSZ (~155µm) | LSCF (25µm) | 850 | | |
| Lohsoontorn et al. [180] | Ni-YSZ; Ni-GDC; Ni/Ru-GDC (30µm) | YSZ (1.5mm) | LSM-YSZ; LSCF; LSF (30µm) | 550-800 | | Ni-YSZ electrode is stable for $H_2O$ electrolysis and hydrogen oxidation, but significantly degraded in $CO_2$ electrolysis and CO oxidation |
| Bercero et al.[a] [153] | Ni-YSZ (400µm) | YSZ (15µm) | LSM/YSZ (20µm) + LSM/YSZ | 750-950 | | Irreversible damage at oxygen electrode-electrolyte interface due to YSZ electrolyte reduction |
| Bercero et al. [152] | Ni-YSZ (~40µm) | 10Sc1CeSZ (155±5µm) | LSCN (~10µm) | 700-850 | | |
| Moyer et al.[a] [182] | Ni-YSZ (1mm) | YSZ (20µm) | LSM-YSZ (10µm) + LSM (20µm) | 750-850 | | |
| Cable et al.[b] [179] | Ni/YSZ (500µm) | YSZ (60µm) | LSCF/YSZ (500µm) | 750-900 | 500 (850℃) | Stable in single mode operation (WE), but degraded in reversible mode operation |
| Jung et al. [183] | Ni-YSZ(720µm) + Ni-YSZ(70µm) | YSZ (18µm) | LSM | 600-800 | | |
| Rao et al. | Ni-BZCY | SDC | SSC-SDC | 700 | | |

| | | | | | | |
|---|---|---|---|---|---|---|
| [184] | | (35μm) | | | | |
| Nguyen et al. [c] [186] | Ni-YSZ | YSZ | LSCF | 750, 760, 810 | | 0.6%/1000h degradation rate at 0.5Acm$^{-2}$ for 4000h FC operation; Negligible degradation at 0.3Acm$^{-2}$ in WE mode |
| Choi et al. [185] | Ni-YSZ; Ni-YSZ + Ni-YSZ | YSZ-GDC | LSCF1982; LSCF1982-GDC | 600-800 | 780 (700℃) 1780 (750℃) 2100 (800℃) | Stable for 72h at 1Acm$^{-2}$ in WE mode, but showed degradation in reversible operation. |
| Su et al. [187] | Ni-YSZ | YSZ (1μm) + GDC(5μm) | LSM-YSZ + LSM/YSZ VAN interlayer | 650-800 | 550 (800℃) 430 (750℃) 320 (700℃) 220 (650℃) | |
| Hong et al.[c] [190] | Ni-YSZ + Ni-YSZ | ScSZ + GDC | LSC-GDC + LSC | 650-800 | | Quite stable in EC mode for 1000h (7.75%/1000h), but rapidly degraded in regenerative operation within 5 cycles (~140h) |
| Fan et al. [189] | Ni-YSZ (300μm) | YSZ(20-30μm)+ GDC(10μm) | LSCF (60-70μm) | 750-850 | 486 (850℃) 401 (800℃) 296 (750℃) | Voltage degradation rate of 2.7% and 5.9% for FC mode and EC mode after alternatively operated at ±300 mAcm$^{-2}$ for 13 cycles (26hrs) |
| Fan et al. [188] | Ni-YSZ (300μm) | YSZ (20-30μm) | LSCF/YSZ (70μm) | 700-800 | 900 (800℃) 640 (700℃) | Voltage degradation rate of 3.4% and 4.9% for FC mode and EC mode after alternatively operated at ±600 mAcm$^{-2}$ for 8 cycles (16hrs) |
| Yoon et al. [191] | Ni-YSZ (800μm) + Ni-YSZ (10μm) | YSZ (10μm) + GDC (5μm) | LSC-GDC (15μm) + LSC (20μm) | 700-800 | 1300 (700℃) 1600 (750℃) 1800 (800℃) | |
| Lee et al. | Ni-YSZ + | YSZ + GDC | SSC/LSCF- | 700- | 1620 | |

| | | | | | | |
|---|---|---|---|---|---|---|
| [160] | Ni-YSZ | | GDC + LSCF | 800 | (750℃) | |
| Molero-Sanchez et al. [b] [194] | LCFCr (30µm) | GDC (1mm) | LCFCr (30µm) | 600-800 | | very stable, with very little loss in performance and no interfacial damage observed after 100 h at a 0.4V (OER) and -0.4V (ORR) overpotentials |
| Chen et al. [192] | Ni-SDC/YSZ (~50µm) | ScSZ (~15µm) | $Nd_2O_3$-$Nd_2NiO_{4+\delta}$/ScSZ (~30µm) | 650-800 | | Cell performance is improved after more than 300hrs' operation in WE mode |
| Yoo et al. [195] | Ni-GDC + Ni-GDC | GDC | LNO | 500-650 | ~190 (650℃) | Stable in FC mode at 0.1Acm$^{-2}$ at 600℃ for 100hrs |
| Ferrero et al. [193] | Ni-YSZ (5-10 µm) + Ni-YSZ (450-550µm) | YSZ (4-6µm) + YDC (2-4µm) | LSM-YSZ (15-30 µm) + LSM (15-30 µm); LSCF(30-60 µm) | 800-850 | | |

[a] Tubular configuration

[b] symmetric cell

[c] Stack

For electrodes, "A-B" means mixed A and B, while "A/B" means A supported on B

**Table-3** RSOFC-H prototypes demonstrated to date

| **References** | **BHE** | **Electrolyte** | **BOE** | **Temp. (℃)** | **PPD ($mWcm^{-2}$)** | **Stability** |
|---|---|---|---|---|---|---|
| Stuart et al. [196] | Pt | BCY10 (450µm) | Pt | 500-750 | | |
| He et al. [197] | Ni-BCZY | BCZY (20µm) | SSC-BCZY (40µm) | 600-700 | 69 (600℃) 140 (650℃) 234 (700℃) | |
| Azimova et al. [198] | Ni/BCZYbCo (100µm) | BCZYbCo (45µm) | LSC-BCZYbCo (20µm) | 600-700 | | |
| Rao et al. [199] | Ni-BCZY | BCZY (20µm) | BZC-0.4 (30µm) | 700 | | Quite stable in EC mode (1.3V) for 5hrs |
| Yoo et al. [200] | Ni-BCZY | BCZY (10-15µm) | BSCF-BCZY (20µm) | 600 | 493 | Relatively stable at $300mAcm^{-2}$ in FC mode for 600hrs |

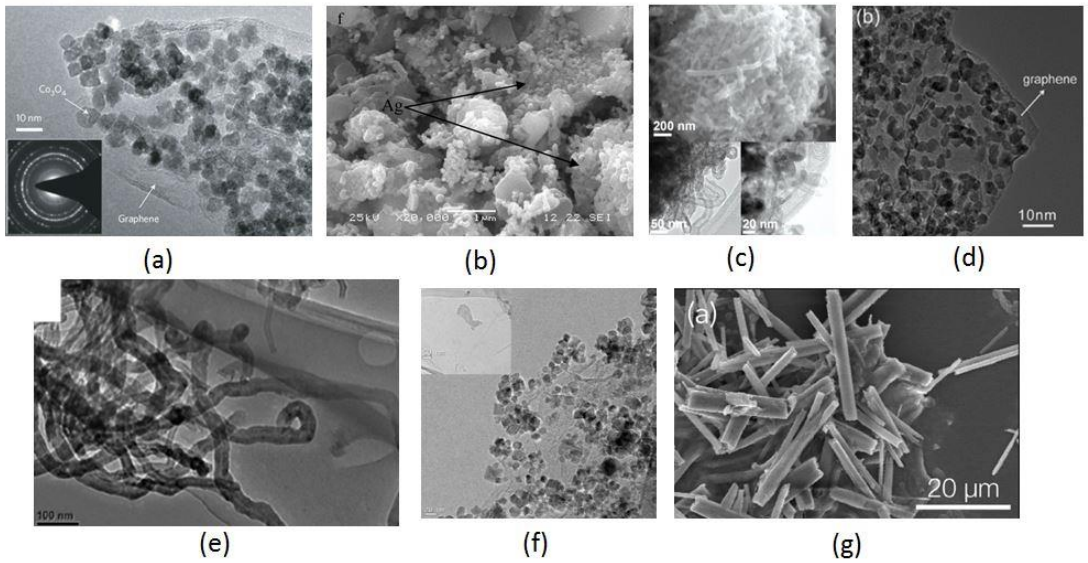


Fig. 1 SEM images of various hybrid BOCs with synergistic effects: (a) $Co_3O_4$/N-rmGO [83]; (b) Ag modified $La_{0.6}Ca_{0.4}CoO_3$ [125]; (c) Core−corona structured $LaNiO_3$-NCNTs [104]; (d) $NiCo_2S_4$@N/S-rGO [120]; (e) B-MWCNTs [63]; (f) $CoMn_2O_4$/N-rGO [95]; (g) $CoC_2O_4$/gRGO [123]

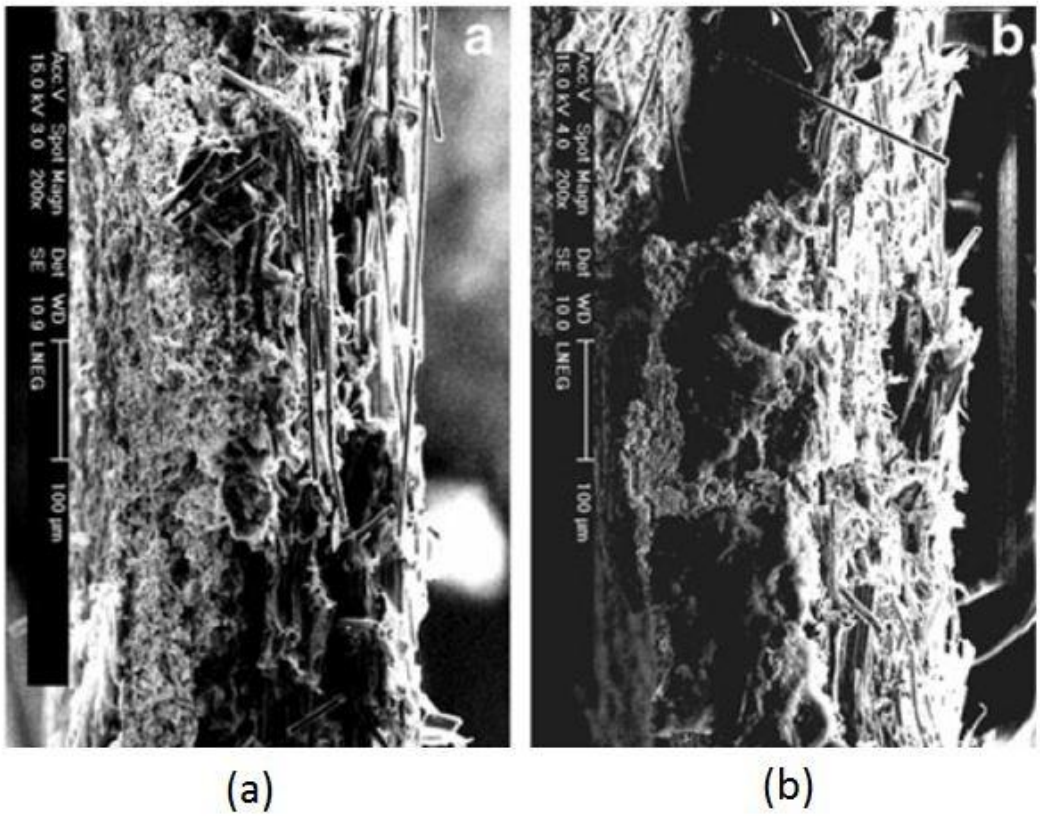


Fig. 2 Evidence of the carbon-based electrode corrosion in alkaline environment [146]: (a) before 200 cycles; (b) after 200 cycles

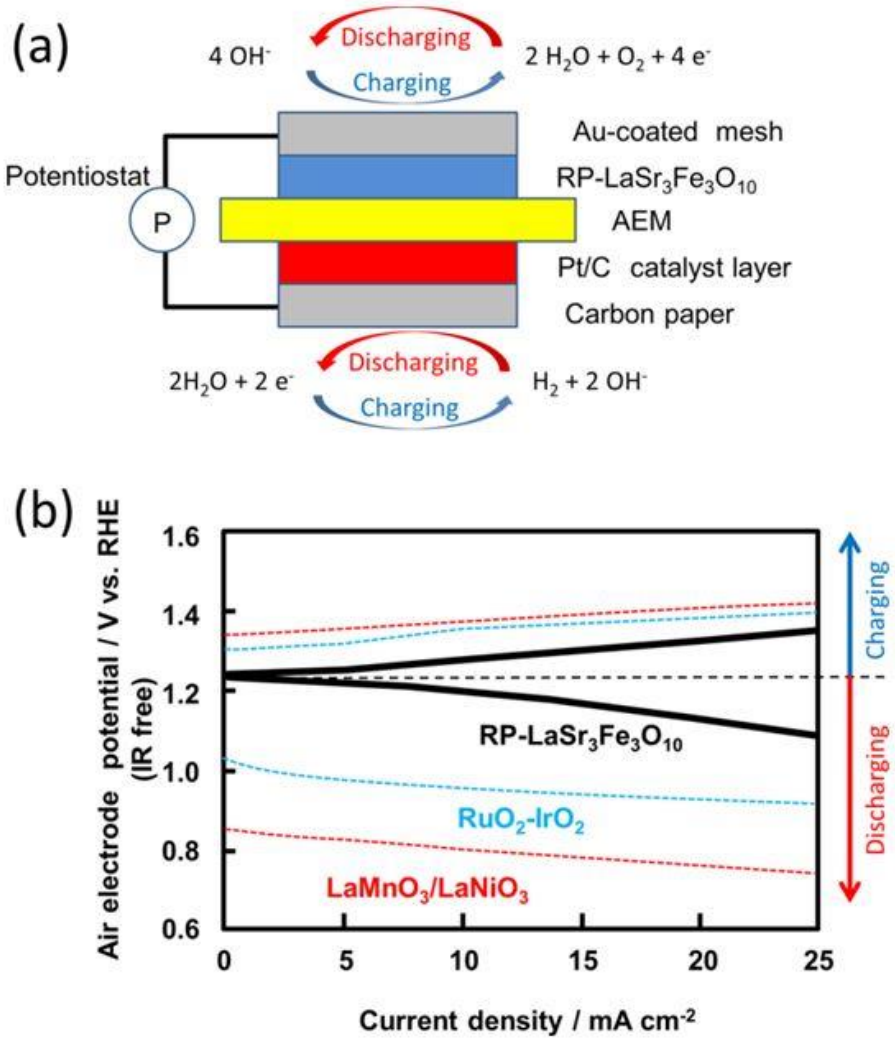


Fig. 3 A UR-AFC based on the RP-$LaSr_3Fe_3O_{10}$ oxygen electrode shows much lower overpotentials in both modes [16]: (a) cell composition; (b) polarization curve

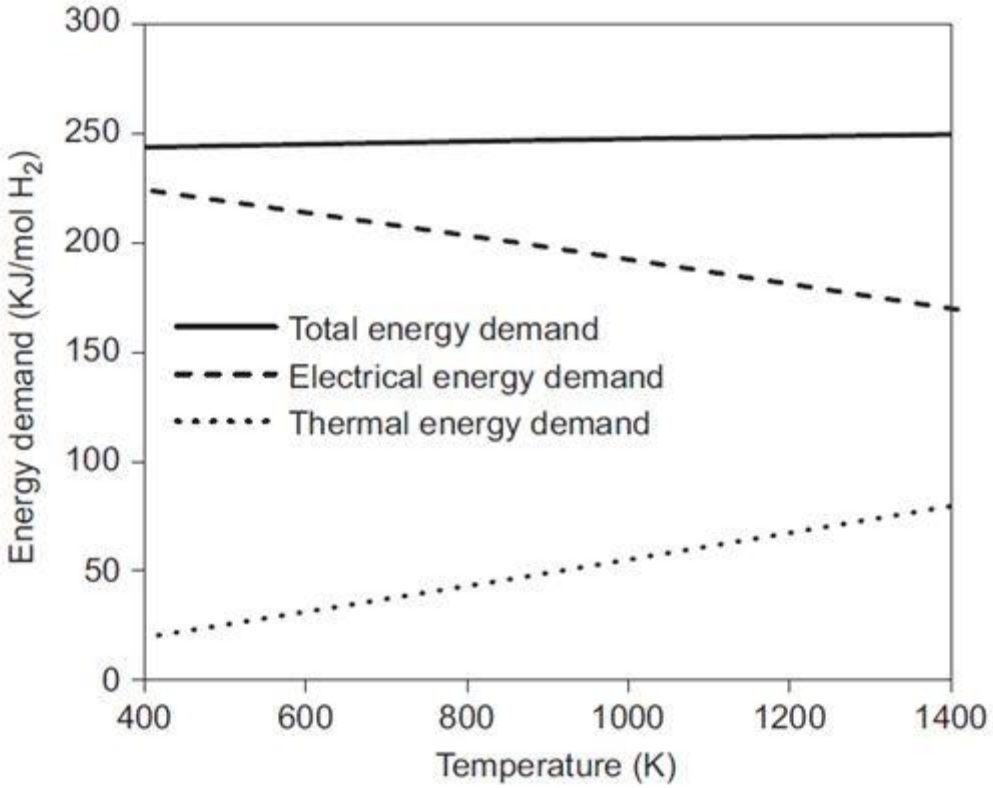


Fig. 4 Calculated energy demand for water electrolysis under various temperatures [154]

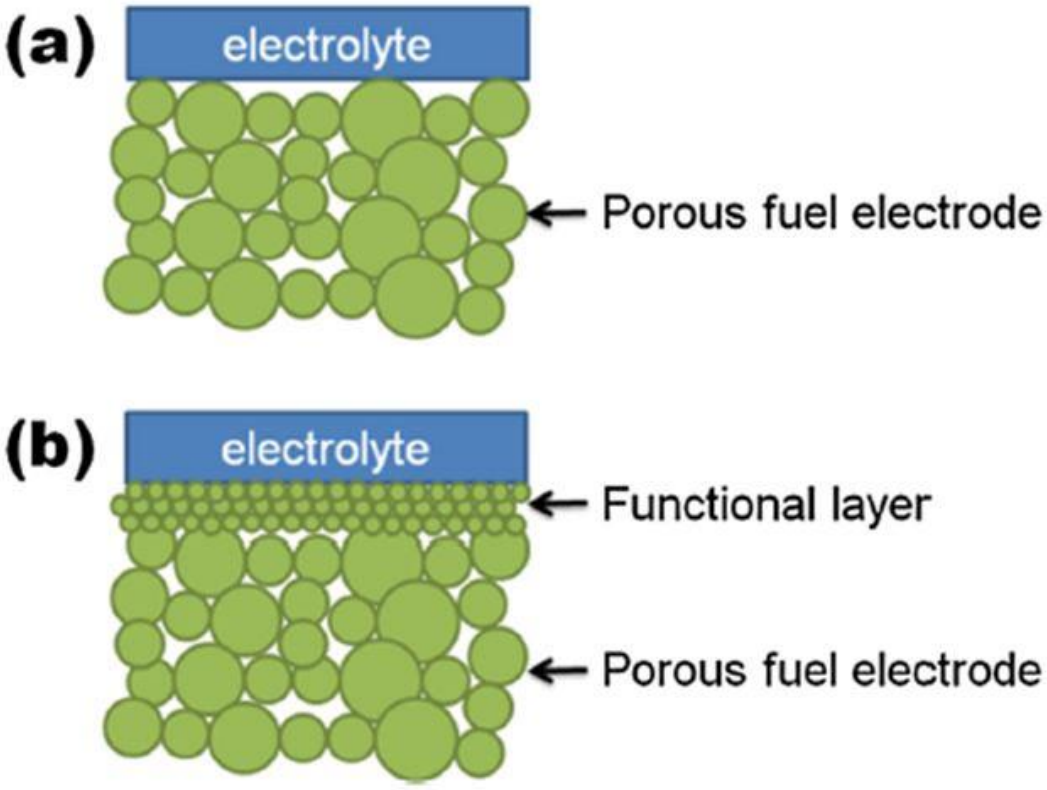


Fig. 5 Schematic diagram of different hydrogen electrode structures [158]: (a) conventional one-layer structure; (b) Two-layer structure

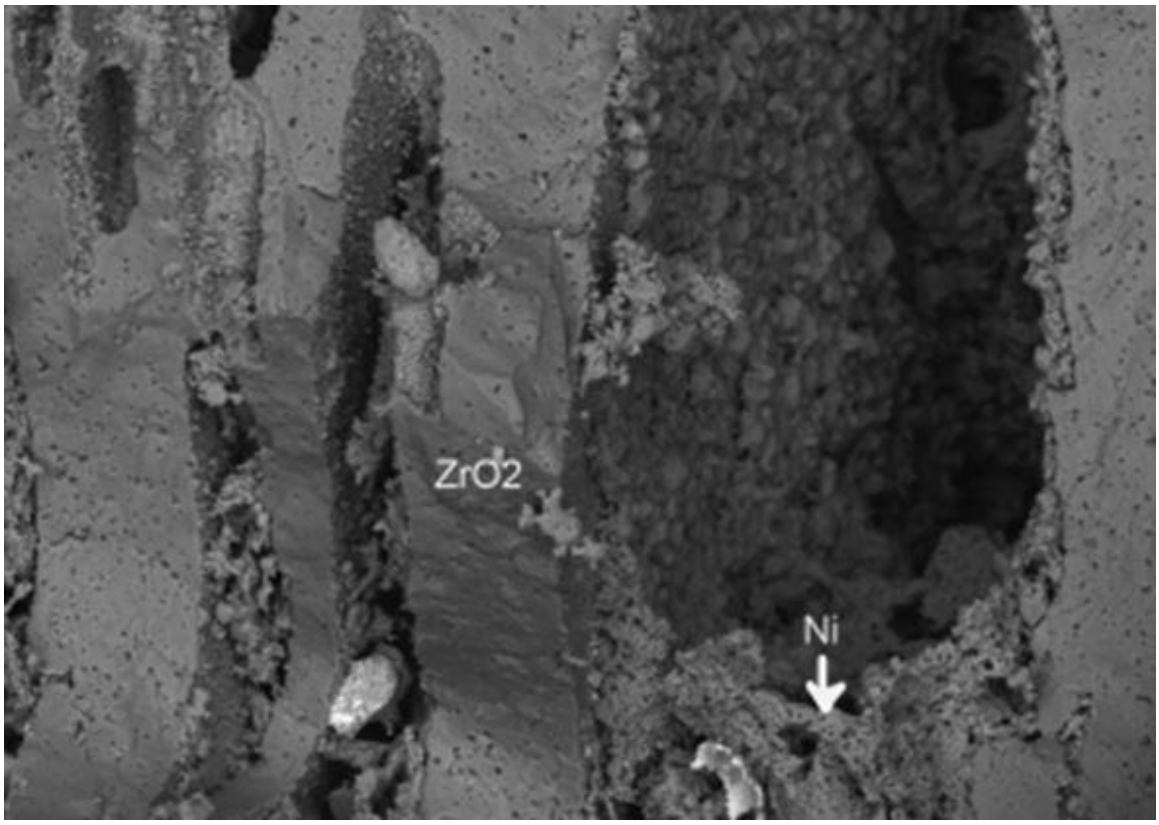

Fig. 6 A novel BHE with Ni particles dispersed in porous YSZ scaffold, which alleviate the Ni agglomeration problem after EC mode operation [179]

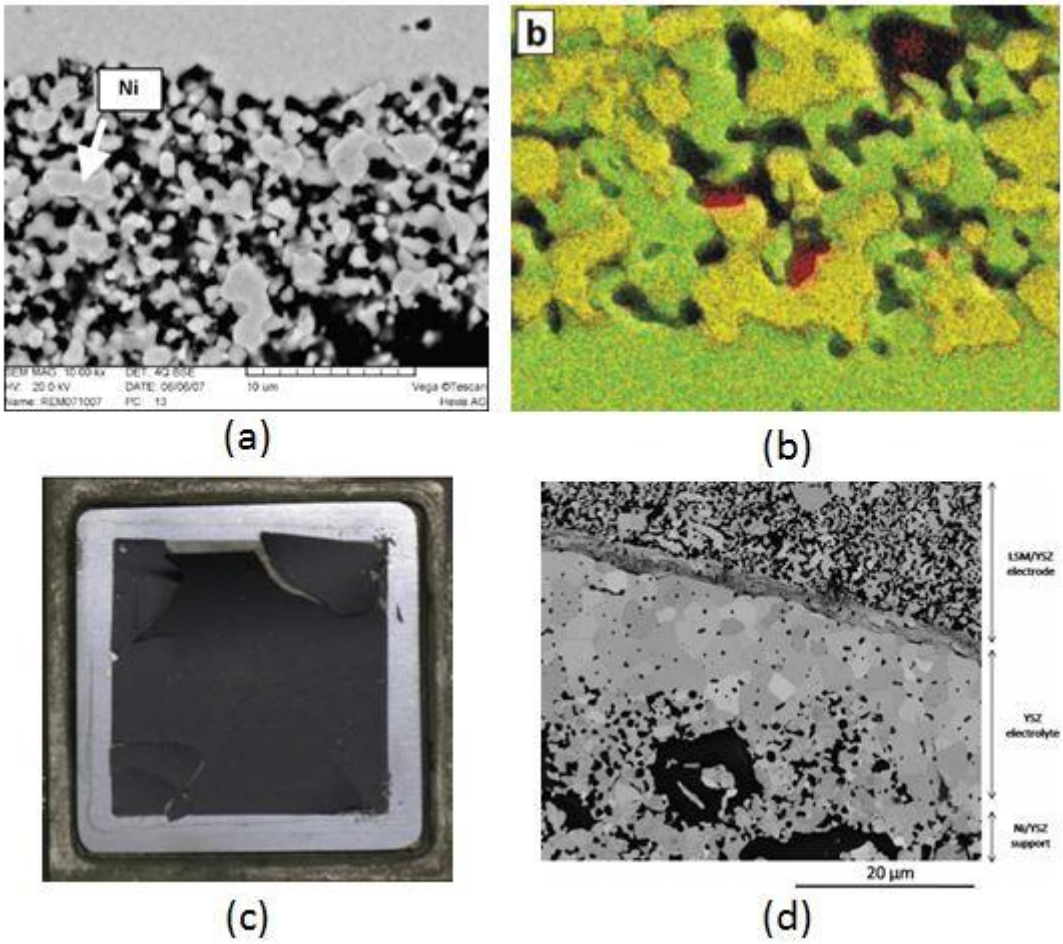


Fig. 7 Major degradation mechanisms to a single RSOFC: (a) Ni particle agglomeration [204]; (b) Si-containing impurities (red) from glass sealants [174]; (c) oxygen electrode delamination [190]; (d) YSZ electrolyte reduction [153]

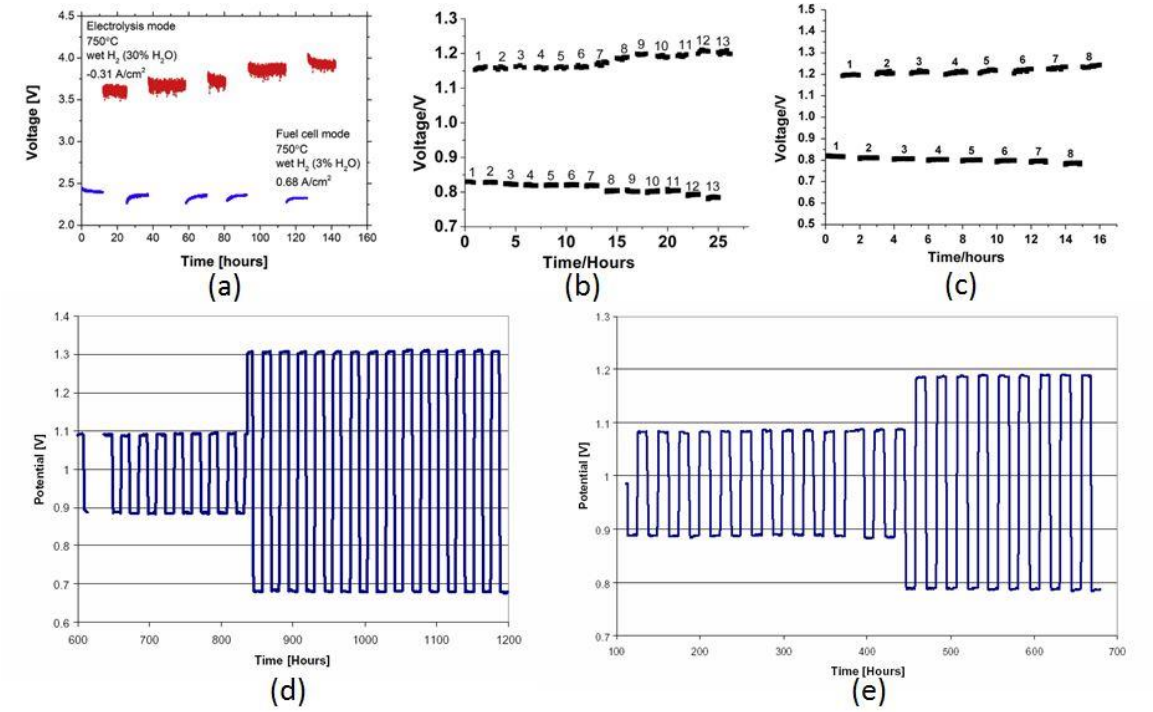


Fig. 8 Stability study of various RSOFCs in regenerative mode operation: (a) From Hong et al. [190] (b)(c) From Fan et al. [188, 189] (d)(e) From McElroy et al. [171]

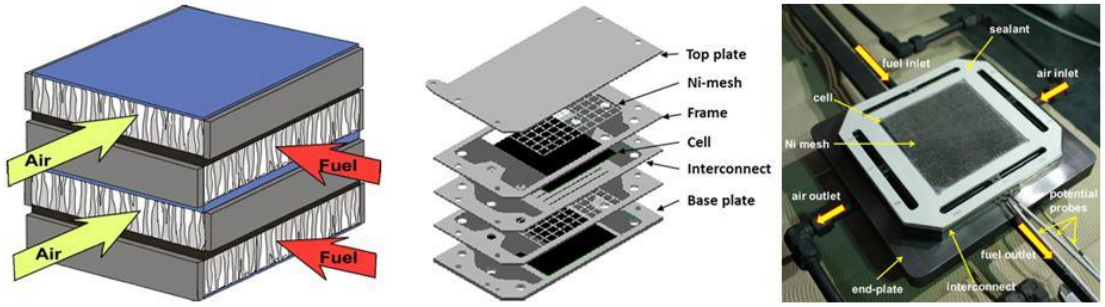


(a) (b) (c)

Fig. 9 RSOFC-O stack prototypes in the literature: (a) NASA all-ceramic stack by Cable et al. [179] (b) Jülich 2-cell stack by Nguyen et al. [186] (c) 200W-class 3-cell stack by Hong et al. [190]

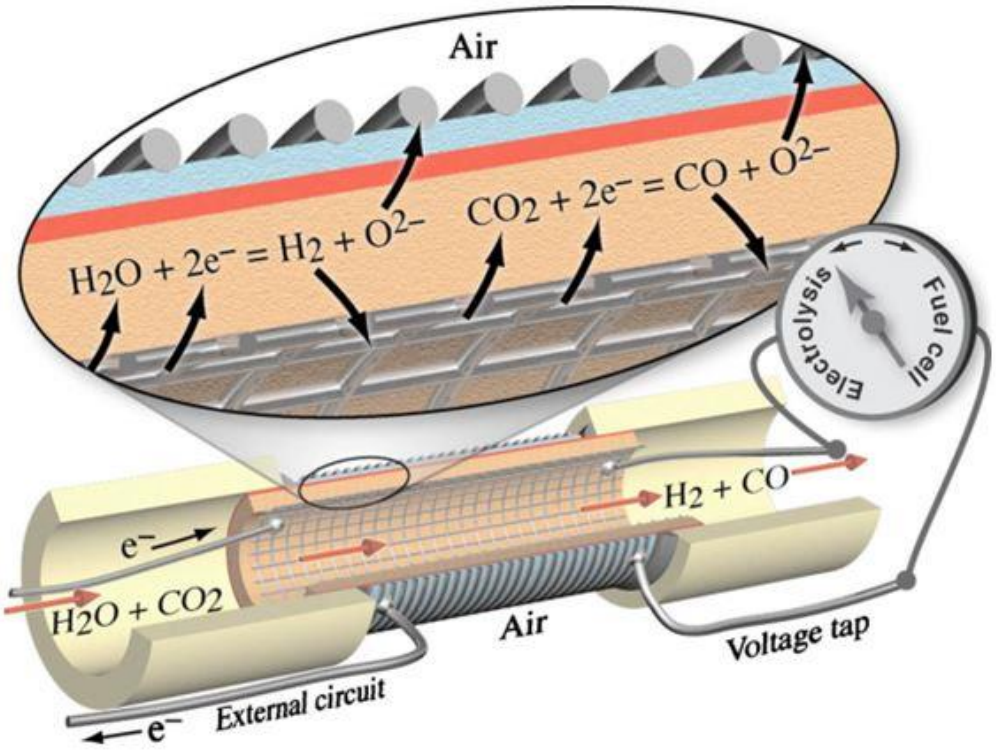


Fig. 10 Micro-tubular RSOFC prototype [182]

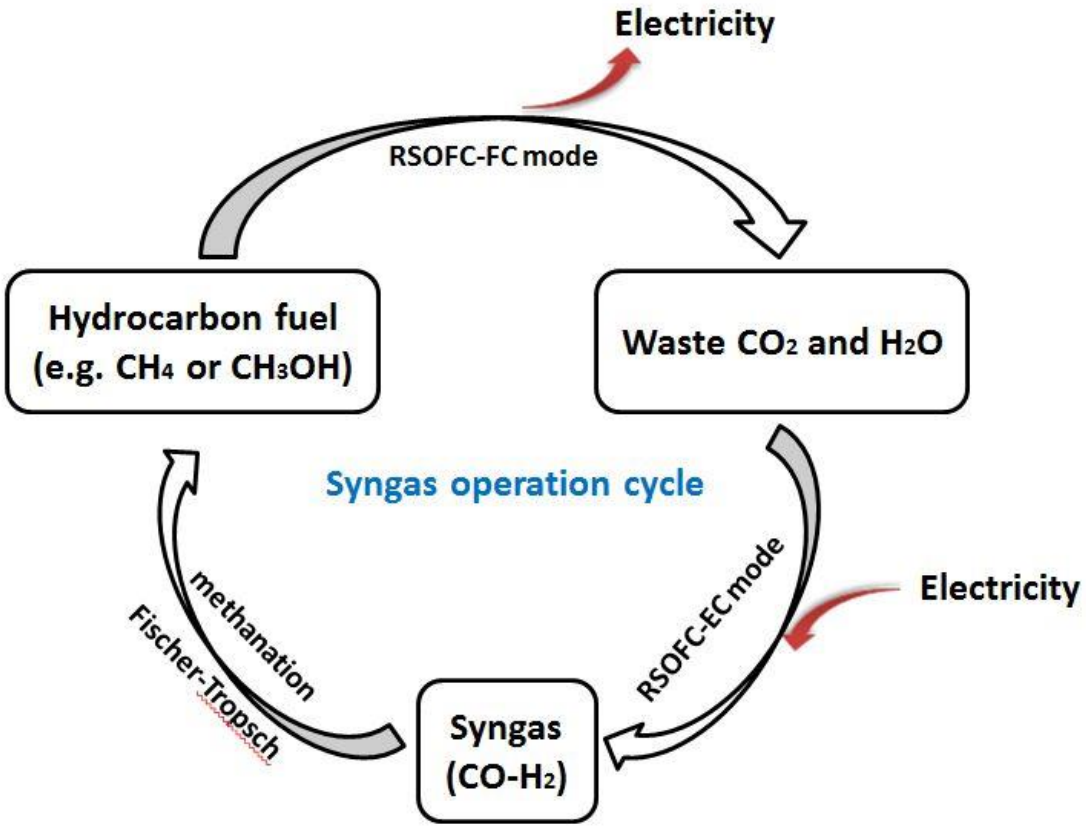


Fig. 11 Schematic diagram of RSOFCs with syngas operation

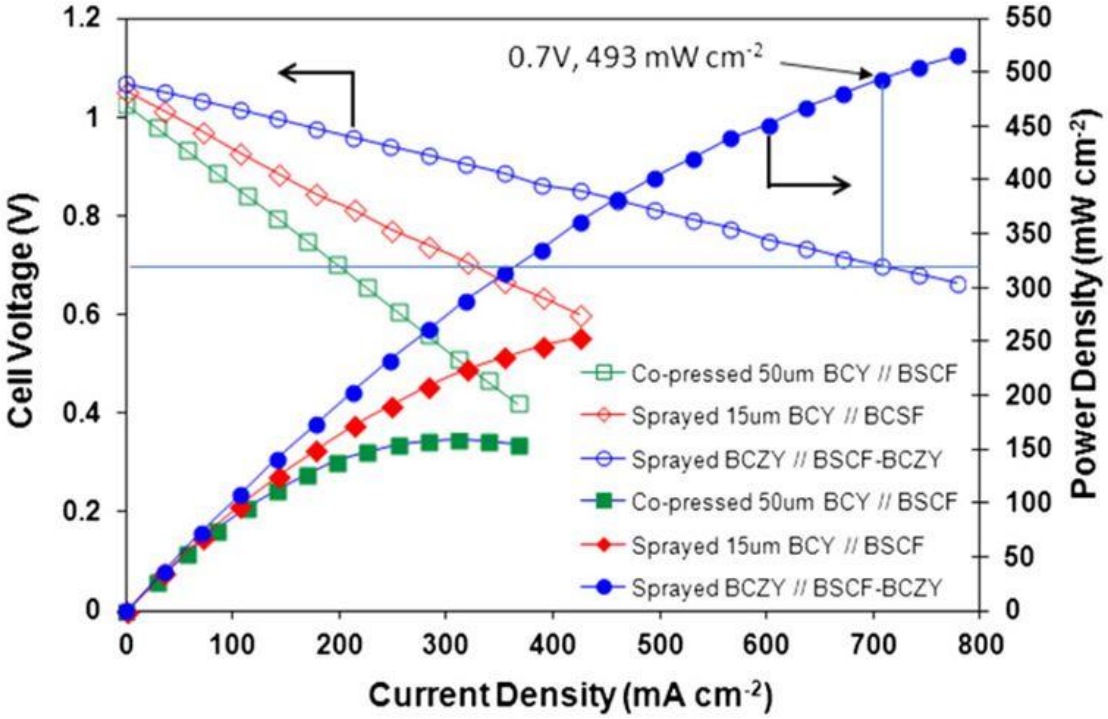


Fig. 12 I-V characteristics of single cells prepared by different fabrication processes and electrolyte materials at 600℃ under humid 75% H2 in Ar (2.76% H2O) and humid air [200]

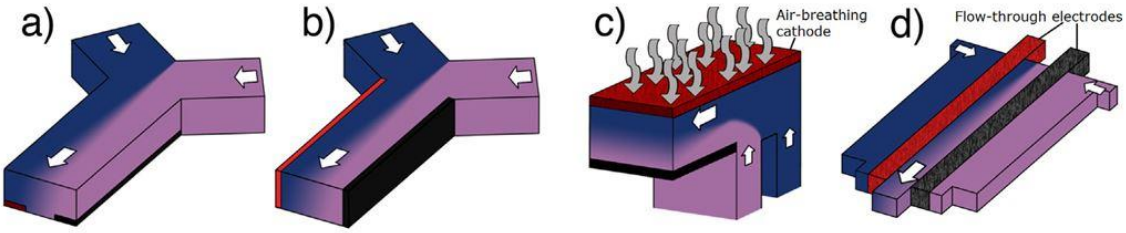


Fig. 13 Microfluidic fuel cells with various structures [9]: (a) T-type with electrodes on the channel bottom; (b) T-type with electrodes on the channel sides; (c) F-type air-breathing cathode; (d) Flow-through electrodes

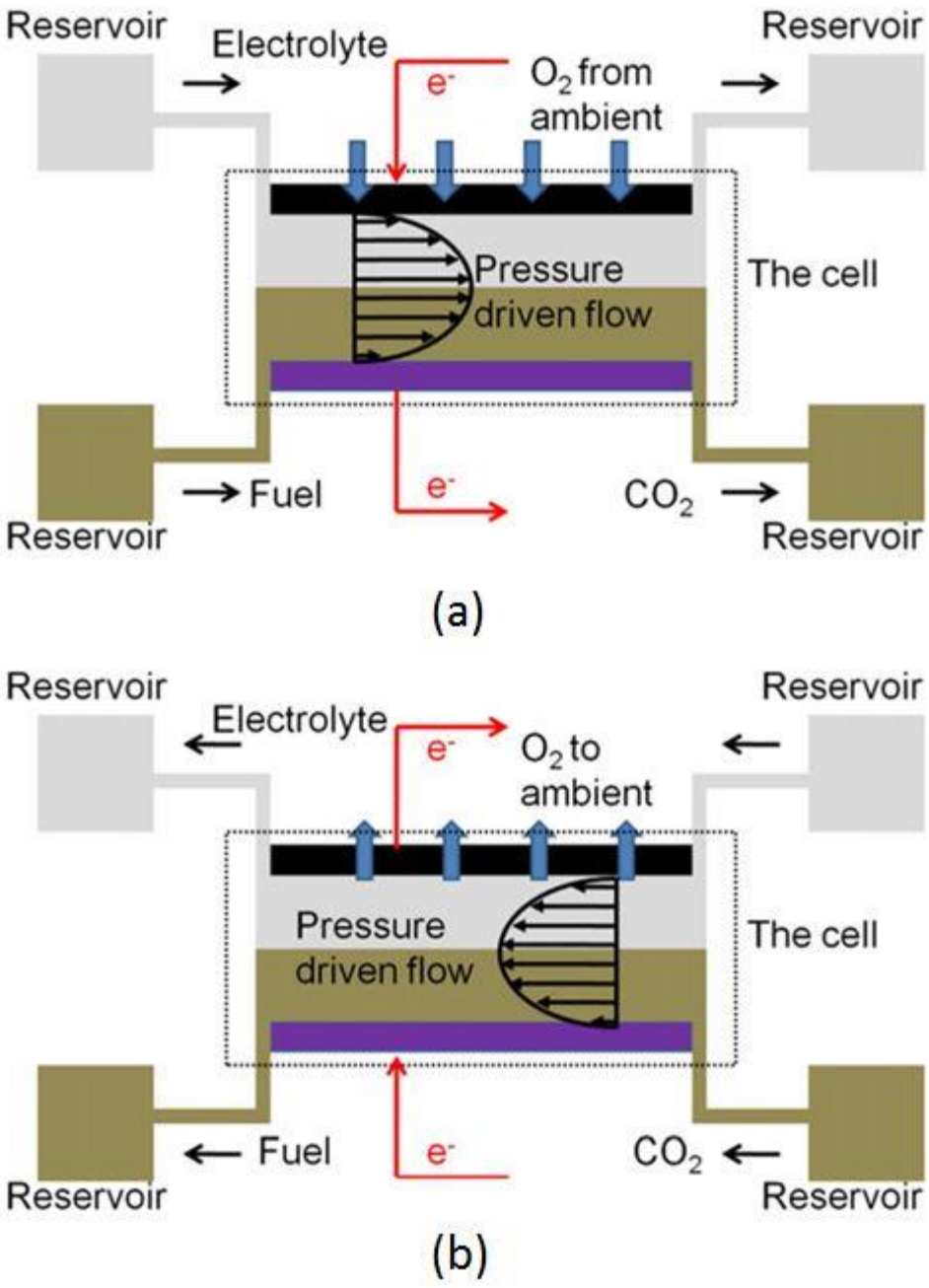


Fig. 14 Schematic diagram of an air-breathing RMFC [247]: (a) FC mode; (b) EC mode